

Donor–Acceptor (Electronic) Coupling in the Precursor Complex to Organic Electron Transfer: Intermolecular and Intramolecular Self-Exchange between Phenothiazine Redox Centers

Duoli Sun, Sergiy V. Rosokha, and Jay K. Kochi*

Contribution from the Department of Chemistry, University of Houston, Houston, Texas, 77204-5003

Received September 26, 2003; E-mail: jkochi@uh.edu

Abstract: Intermolecular electron transfer (ET) between the free phenothiazine donor (PH) and its cation radical (PH^{•+}) proceeds via the [1:1] precursor complex (PH)₂^{•+} which is transiently observed for the first time by its diagnostic (charge-resonance) absorption band in the near-IR region. Similar intervalence (optical) transitions are also observed in mixed-valence cation radicals with the generic representation: P(br)P^{•+}, in which two phenothiazine redox centers are interlinked by *p*-phenylene, *o*-xylylene, and *o*-phenylene (br) bridges. Mulliken–Hush analysis of the intervalence (charge-resonance) bands afford reliable values of the electronic coupling element H_{IV} based on the separation parameters for (P/P^{•+}) centers estimated from some X-ray structures of the intermolecular (PH)₂^{•+} and the intramolecular P(br)P^{•+} systems. The values of H_{IV}, together with the reorganization energies λ derived from the intervalence transitions, yield activation barriers ΔG_{ET}[‡] and first-order rate constants k_{ET} for electron-transfer based on the Marcus–Hush (two-state) formalism. Such theoretically based values of the intrinsic barrier and ET rate constants agree with the experimental activation barrier (E_a) and the self-exchange rate constant (k_{SE}) independently determined by ESR line broadening measurements. This convergence validates the use of the two-state model to adequately evaluate the critical electronic coupling elements between (P/P^{•+}) redox centers in both (a) intermolecular ET via the precursor complex and (b) intramolecular ET within bridged mixed-valence cation radicals. Important to intermolecular ET mechanism is the intervention of the strongly coupled precursor complex since it leads to electron-transfer rates of self-exchange that are 2 orders of magnitude faster (and activation barrier that is substantially lower) than otherwise predicted solely on the basis of Marcus reorganization energy.

Introduction

Classical Marcus theory has been successfully applied to the prediction of intrinsic (activation) barriers, i.e., reorganization energies λ, of various self-exchange reactions and to electron-transfer (ET) rates of cross-exchange reactions from knowledge of the component self-exchanges, especially of transition-metal (inorganic) redox processes.^{1–3} The subsequent extension of Marcus theory to conventional organic and organometallic donor and acceptor dyads was lately summarized by Ebersson⁴ in the ground-breaking and widely cited monograph, *Electron-Transfer Reactions in Organic Chemistry*. At the crux of the theoretical treatment is the evaluation of the intrinsic ET barrier for experimental self-exchange rates that generally are obtained

from stopped flow and EPR line broadening measurements pertinent to paramagnetic redox centers. However, when the quantitative applicability of classical Marcus theory was later tested in a direct comparison of experimental and theoretical activation barriers for organic self-exchange reactions, the calculated barriers were actually found in many cases to be significantly higher than otherwise expected.⁵ The possible origin of such a discrepancy between theory and experiment was recently traced by Nelsen and Pladziewicz⁶ to the inherent limitation of classical Marcus theory to redox systems with restricted values of the electronic coupling between the donor and acceptor dyads, generally with the electronic coupling element (H_{DA}) < 200 cm⁻¹.^{2,7}

According to Sutin,^{2,8} the generalized expression for the Marcus activation barrier can be alternatively expressed as eq 1 to accommodate those redox systems with substantive values

$$\Delta G^{\ddagger} = (\lambda - 2H_{DA})^2/4\lambda \quad (1)$$

of H_{DA}, i.e., adiabatic (strongly coupled) systems. (As such, eq

- (1) (a) Marcus, R. A. *Angew. Chem., Int. Ed. Engl.* **1993**, *32*, 1111. (b) Marcus, R. A. *Discuss. Faraday Soc.* **1960**, *29*, 21. (c) Marcus, R. A. *J. Phys. Chem.* **1963**, *67*, 853. (d) Marcus, R. A. *J. Chem. Phys.* **1965**, *43*, 679. (e) Marcus, R. A.; Sutin, N. *Biochim. Biophys. Acta* **1985**, *811*, 265.
- (2) Sutin, N. *Prog. Inorg. Chem.* **1983**, *30*, 441.
- (3) (a) Newton, M. D. In *Electron Transfer in Chemistry*; Balzani, V., Ed.; Wiley-VCH: New York, 2001; Vol. 1, p 3. (b) Astruc, D. *Electron Transfer and Radical Processes in Transition-Metal Chemistry*; Wiley-VCH: New York, 1995. (c) Cannon, R. D. *Electron-Transfer Reactions*; Butterworth: London, 1980.
- (4) Ebersson, L. *Electron-Transfer Reactions in Organic Chemistry*; Springer-Verlag: New York, 1987.

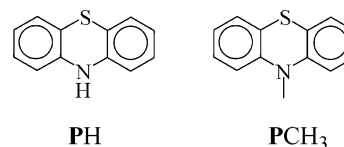
- (5) Ebersson, L.; Shaik, S. S. *J. Am. Chem. Soc.* **1990**, *112*, 4484.
- (6) Nelsen, S.; Pladziewicz, J. *Acc. Chem. Res.* **2002**, *35*, 247.

1 attains the classical Marcus limit of $\Delta G^\ddagger = \lambda/4$ only when $\lambda \gg H_{DA}$.) Thus, the inclusion of H_{DA} (initially) as a disposable parameter by Nelsen and Pladziewicz⁶ of a large and diverse number of experimentally measured cross-exchange reactions led to consistently good correlations with theoretically evaluated (self-consistent) sets of intrinsic barriers based on eq 1.

This important finding raises a number of interesting questions about organic/organometallic electron-transfer processes. First, what is the mechanistic significance of the electronic coupling element when the composite term $\lambda - 2H_{DA}$ is notably less than λ ? Second, how do such substantial values of the electronic coupling element experimentally impinge on the quantitative evaluation of the effective activation barrier for intermolecular ET? Critical to addressing these questions is the independent experimental measurement of the electronic coupling element. In this study, we focus on a single redox center, the phenothiazinyl group (**P**), because of the reversible oxidation of this rather extended aromatic group to generate its persistent cation radical ($\mathbf{P}^{\bullet+}$) at the accessible potential of only $E_{ox}^\circ = 0.61$ V vs SCE.^{9,10} Our choice of the phenothiazinyl redox center in a more general context relates to its extensive use in a variety of intermolecular and intramolecular thermal and photochemical redox processes primarily aimed at development and testing of different aspects of electron-transfer theory,¹¹ to its mimicking biochemical (redox) processes,¹² as well as to its bearing on organic and organometallic material science.¹³

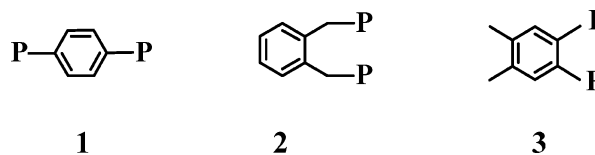
For intermolecular ET, we reexamine the electron-transfer kinetics between the parent phenothiazine donor (**PH**) and its cation radical ($\mathbf{PH}^{\bullet+}$) as well as that of its *N*-methyl derivative in Chart 1 that were originally delineated by Bard and

Chart 1



co-workers,¹⁴ but now with particular attention to the transient appearance of diagnostic intervalence (charge resonance, CR) absorption bands of the precursor complex heretofore unreported. Intramolecular electron exchange between phenothiazinyl redox centers is then identified in mixed-valence cation radicals in which **P** and $\mathbf{P}^{\bullet+}$ are interconnected by three types of molecular bridges, viz. *para*-phenylene, *ortho*-xylylene, and *ortho*-phenylene in the mixed-valence donors **1**, **2**, and **3** depicted in Chart 2, and the direct relationship between intermolecular and intramolecular electron exchange between these ($\mathbf{P/P}^{\bullet+}$) centers is made through the common observation of diagnostic intervalence absorption bands in their electronic spectra.

Chart 2



Results

I. Intermolecular ET Between Phenothiazine and Its Cation Radical. A. Isolation and (UV–Vis/ESR) Characterization of Pure Phenothiazine Cation Radical. Selective oxidation of phenothiazine (**PH**) was readily carried out in dichloromethane with 1 equiv of the (one-electron) oxidant tris-(4-bromophenyl) aminium hexachloroantimonate¹⁵ to afford the pure cation radical $\mathbf{PH}^{\bullet+}$ as the brown crystalline SbCl_6^- salt (see Experimental Section).¹⁶ The red crystalline salt of the corresponding *N*-methyl derivative $\mathbf{PMe}^{\bullet+}\text{SbCl}_6^-$ was prepared by the same procedure.

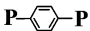
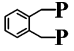
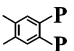
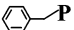
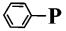
The electronic spectrum of the phenothiazine cation radical salt dissolved in dichloromethane is characterized by three groups of bands: (a) local (UV) absorptions at 272 and 320 nm that are related to those at 255 and 316 nm in the parent phenothiazine,¹⁷ (b) prominent (vis) bands at 437 and 519 nm that are absent in the parent donor, and (c) weak (near-IR) bands listed in Table 1, together with those of the *N*-methyl analogue $\mathbf{PMe}^{\bullet+}$. The resolved ESR spectrum of phenothiazine cation radical (Figure S1, Supporting Information) was well-simulated for this study using the hyperfine splitting constants established earlier.¹⁸

B. Concentration-Dependent ESR Line Broadening and Self-Exchange Rates between Phenothiazine Donor and Acceptor Couples. The incremental addition of free phenothi-

- (7) (a) Such an upper limit of the electronic coupling element is rather arbitrary since it depends on the reorganization energy. See: Nelsen, S. In *Electron Transfer in Chemistry*, Balzani, V., Ed.; Wiley-VCH: New York, 2001; Vol. 1, p 342. (b) As used here, H_{DA} emphasizes the molecular-orbital description of the electronic coupling element between the donor and acceptor in the precursor complex, whereas the more conventional H_{ab} is based on the valence bond description of electronic coupling between the initial and final (ET) diabatic states. Their theoretical equivalence has been quantitatively demonstrated by Newton^{3a} and underscores another example of the never-ending rivalry between MO and VB treatments. See: Hoffmann, R.; Shaik, S.; Hiberty, P. C. *Acc. Chem. Res.* **2003**, *36*, 750. (8) (a) Brunschwig, B. S.; Sutin, N. In *Electron Transfer in Chemistry*, Balzani, V., Ed.; Wiley-VCH: New York, 2001; Vol. 1, p 583. (b) Brunschwig, B. S.; Sutin, N. *Coord. Chem. Rev.* **1999**, *187*, 233. (c) Sutin, N. *Adv. Chem. Phys.* **1999**, *106*, 7. (d) Cretz, C.; Newton, M. D.; Sutin, N. *J. Photochem. Photobiol., A* **1994**, *82*, 47. (9) See Ebersson in ref 4, p 44. (10) Moreover, the sizable reorganization energy for this redox pair derives from a significant configurational change of the tub-shaped **P** to the planar $\mathbf{P}^{\bullet+}$ attendant upon one-electron oxidation. The latter also points to the mechanistic advantage accrued in a more general context by the use of "infinitely" variable organic structures for electron-transfer studies. (11) (a) Chen, P.; Duesing, R.; Graff, D. K.; Meyer, T. J. *J. Phys. Chem.* **1991**, *95*, 5850. (b) Ohno, T.; Yoshimura, A.; Mataga, N. *J. Phys. Chem.* **1990**, *94*, 4871. (c) Pelizzetti, E.; Giordano, R. *J. Chem. Soc., Dalton Trans.* **1979**, 1516. (d) Sorensen, S. P.; Bruning, W. H. *J. Am. Chem. Soc.* **1973**, *95*, 2445. (e) Nath, S.; Singh, A. K.; Palit, D. K.; Sapre, A. V.; Mittal, J. P. *J. Phys. Chem. A* **2001**, *105*, 7151. (f) Daub, J.; Engl, R.; Kurzawa, J.; Miller, S. E.; Schneider, S.; Stockmann, A.; Wasielewski, M. R. *J. Phys. Chem. A* **2001**, *105*, 5655. (g) Shimada, E.; Nagano, M.; Iwahashi, M.; Mori, Y.; Sakaguchi, Y.; Hayashi, H. *J. Phys. Chem. A* **2001**, *105*, 2997. (h) Reid, G. D.; Whittaker, D. J.; Day, M. A.; Creely, C. M.; Tuite, E. M.; Kelly, J.; Beddard, G. S. *J. Am. Chem. Soc.* **2001**, *123*, 6953. (i) Larson, S. L.; Elliott, C. M.; Kelley, D. F. *Inorg. Chem.* **1996**, *35*, 2070. (j) Larson, S. L.; Cooley, L. F.; Elliott, C. M.; Kelley, D. F. *J. Am. Chem. Soc.* **1992**, *114*, 9504. (k) Borowitz, P.; Herbich, J.; Kapturkiewicz, A.; Opallo, M.; Nowacki, J. *Chem. Phys.* **1999**, *249*, 49. (l) Kramer, C. S.; Zeutler, K.; Müller, T. J. *J. Tetrahedron Lett.* **2001**, *49*, 8619. (12) (a) Kawai, K.; Takada, T.; Tojo, S.; Majima, T. *J. Am. Chem. Soc.* **2003**, *125*, 6842. (b) Shen, Z.; Strauss, J.; Daub, J. *Chem. Commun.* **2002**, 460. (c) Koenig, B.; Pelka, M.; Zieg, H.; Ritter, T.; Bouas-Laurent, H.; Bonneau, R.; Desvergne, J.-P. *J. Am. Chem. Soc.* **1999**, *121*, 1681. (13) (a) Fungo, F.; Samson, A.; Bard, A. J. *Chem. Mater.* **2003**, *15*, 1264. (b) Ehmann, A.; Gompper, R.; Hartmann, H.; Mueller, T. J. J.; Polborn, K.; Schuetz, R. *Angew. Chem., Int. Ed. Engl.* **1994**, *33*, 572. (c) Margerum, L. D.; Murray, R. W.; Meyer, T. J. *J. Phys. Chem. A* **1986**, *90*, 728.

- (14) Kowert, B. A.; Marcoux, B. A.; Bard, A. J. *J. Am. Chem. Soc.* **1972**, *94*, 5538. (15) (a) Bell, F. A.; Ledwith, A.; Sherrington, D. C. *J. Chem. Soc. C* **1969**, 2719. (b) Connelly, N. G.; Geiger, W. E. *Chem. Rev.* **1996**, *96*, 877. (16) The rather large SbCl_6^- was consistently used as a relative noncoordinating anion to minimize electrostatic effects of the counterion on $\mathbf{PH}^{\bullet+}$ and $\mathbf{PMe}^{\bullet+}$ in the ET and self-association processes. (17) (a) Shine, H. J.; Mach, E. E. *J. Org. Chem.* **1965**, *30*, 2130. (b) Wagner, E.; Filipek, S.; Kalinowski M. K. *Monatsh. Chem.* **1988**, *119*, 929. (18) Lu, J.-M.; Chen, Y.; Wen, X.; Wu, L.-M.; Jia, X.; Liu, Y. C.; Liu, Z.-L. *J. Phys. Chem. A* **1999**, *103*, 6998.

Table 1. Electronic Spectra (in the NIR region) of Cation Radicals (CR) and Dication (DC) of Phenothiazine-Based Mixed-Valence Donors and Their Mononuclear Models^a

| Donor | CR or DC | Wavelength, nm (ϵ , $10^3\text{M}^{-1}\text{cm}^{-1}$) |
|---|-------------------|---|
| P-H | PH ^{•+} | 675sh 736(0.79) 830(0.72) |
| PMe | PMe ^{•+} | 701sh 772(1.4) 867(1.4) |
|  | 1 ^{•+} | 679sh 781(0.95) 885(0.72) 943(0.36) ^b |
| | 1 ²⁺ | 690sh 793(1.9) 892(1.4) |
|  | 2 ^{•+} | 674sh 775(0.96) 870(0.65) 910(0.86) ^b |
| | 2 ²⁺ | 680sh 809(1.9) 915(1.5) |
|  | 3 ^{•+} | 700sh 803(0.7) 905 (0.9) 1700 (2.5) |
| | 3 ²⁺ | 794(12.0) |
|  | 4 ^{•+} | 679sh 781(1.4) 885(1.5) |
|  | 5 ^{•+} | 674sh 775(1.3) 870(1.5) |

^a In dichloromethane. ^b Determined by digital deconvolution of spectrum.

azine donor (PH) to a dichloromethane solution of its cation radical (PH^{•+}) resulted in the progressive change in the ESR line widths as previously reported by Bard and co-workers¹⁴ to derive from intermolecular ET between (PH/PH^{•+}) dyads, in which the initial broadening due to slow exchange evolves (upon subsequent narrowing) to approach the fast-exchange limit (Figure S2). Following the earlier kinetic studies, we determined the second-order rate constant in the fast-exchange limit from the line width dependence on the phenothiazine concentration in dichloromethane solution¹⁹ (Figure S3) as $k_{SE} = 5 \times 10^9 \text{ M}^{-1} \text{ s}^{-1}$ for the (PH/PH^{•+}) couple and as $k_{SE} = 1.3 \times 10^9 \text{ M}^{-1} \text{ s}^{-1}$ for the (PMe/PMe^{•+}) couple at 25 °C (see Experimental Section).²⁰ The effective activation barrier of $E_a = 2.2 \text{ kcal mol}^{-1}$ and pre-exponential factor $\log A = 11.3$ were found for the (PH/PH^{•+}) self-exchange from the temperature dependence of k_{SE} (Figure S4).

C. Intervalence (Optical) Transition and the Intermolecular Association of Phenothiazine and Its Cation Radical.

Various mixtures of phenothiazine and phenothiazine cation radical in dichloromethane were characterized by the consistent appearance of a new (unique) absorption band in the near-IR region at 1600 nm under conditions in which neither pure donor (PH) nor pure cation radical (PH^{•+}) showed any absorption, even at high concentrations and low temperatures (vide supra). By contrast, the intensity of the NIR absorption band increased linearly with the concentration of added phenothiazine at a constant (low) concentration of the phenothiazine cation radical (Figure 1), and the new NIR band increased monotonically as the temperature of the (PH/PH^{•+}) solution was progressively lowered. Moreover, computer simulation of the near-IR band confirmed its Gaussian band shape (Figure 1, inset). Such behavior of the extremely red-shifted band with very broad and weak absorbance was reminiscent of the CR transition in the

(19) Note that in this study, dichloromethane was the solvent of choice because of the expanded temperature range accessible for the kinetic studies as well as the enhanced solubility and stability of the various phenothiazine cation radical salts examined in this study.

(20) In acetonitrile solution, self-exchange rate constants of $k_{SE} = 6.7 \times 10^9$ and $2.2 \times 10^9 \text{ M}^{-1} \text{ s}^{-1}$ were determined for PH/PH^{•+} and PMe/PMe^{•+}, respectively, by Bard et al.¹⁴

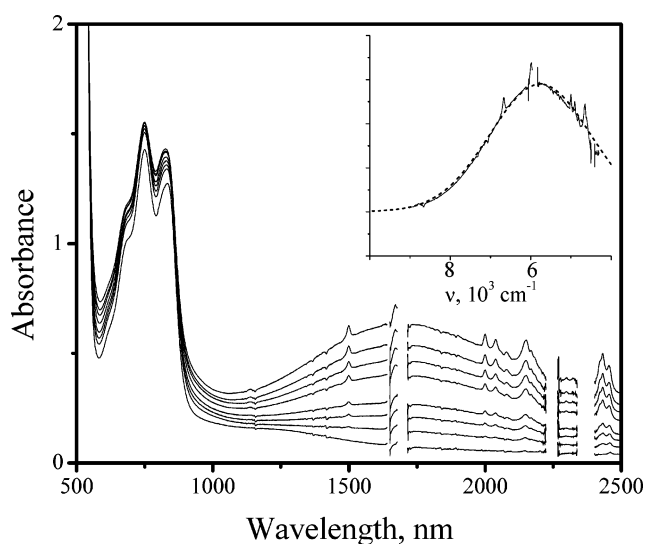
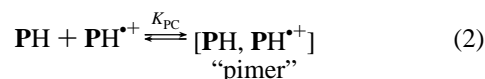


Figure 1. Spectral changes attendant upon the addition of neutral phenothiazine to the dichloromethane solution of its cation radical. Concentrations: PH^{•+} = 2 mM, PH (from bottom to top) = 0, 9, 18 27, 47, 58, 72, 92 mM. Inset: Gaussian deconvolution (dashed line) of the NIR band.

dimer cation radical or paramagnetic pimer derived from the intermolecular association of various aromatic donors with their own cation radical,^{21–23} which in the case of phenothiazine was represented by the reversible equilibrium:



Quantitative analysis of the spectral changes was successfully carried out by the Benesi–Hildebrand methodology,²⁴ i.e., $[\text{PH}^{\bullet+}]/A_{PC} = 1/\epsilon_{PC} + 1/(K_{PC}\epsilon_{PC}[\text{PH}])$, where A_{PC} is the absorbance and ϵ_{PC} is the molar extinction coefficient of the NIR band of the paramagnetic pimer at the monitoring wavelength, and $[\text{PH}^{\bullet+}]$ and $[\text{PH}]$ were the initial concentrations of the phenothiazine cation radical and the parent donor, respectively. The plot of $[\text{PH}^{\bullet+}]/A_{PC}$ versus reciprocal concentration of added $[\text{PH}]$ was linear, and the least-squares fit produced a correlation coefficient of greater than 0.999. The values of the association constant of $K_{PC} = 5 \text{ M}^{-1}$ and extinction

(21) For previous examples of intermolecular π -association of various cation radicals, see: (a) Lewis, L. C.; Singer, L. S. *Chem. Phys.* **1965**, *43*, 2712. (b) Howarth, O. W.; Fraenkel, G. K. *J. Am. Chem. Soc.* **1966**, *88*, 4514. (c) Howarth, O. W.; Fraenkel, G. K. *J. Chem. Phys.* **1970**, *52*, 6258. (d) Badger, B.; Brocklehurst, B. *Nature* **1968**, *219*, 263. (e) Badger, B.; Brocklehurst, B.; Dudley, R. *Chem. Phys. Lett.* **1967**, *1*, 122. (f) Badger, B.; Brocklehurst, B. *Trans. Faraday Soc.* **1969**, *65*, 2582. (g) Badger, B.; Brocklehurst, B. *Trans. Faraday Soc.* **1969**, *65*, 2588. (h) Badger, B.; Brocklehurst, B. *Trans. Faraday Soc.* **1970**, *66*, 2939. (i) Meot-Ner, M.; Hamlet, P.; Hunter, E. P.; Field, F. H. *J. Am. Chem. Soc.* **1978**, *100*, 5466. (j) Meot-Ner, M. *J. Phys. Chem.* **1980**, *84*, 2724. (k) Meot-Ner, M.; El-Shall, M. S. *J. Am. Chem. Soc.* **1986**, *108*, 4386. (l) All attempts to prepare the corresponding anionic dimers in solution have been unsuccessful heretofore. (m) Since the cationic and anionic dimers are both derived from π -donor/acceptor pairs, they are hereinafter referred to interchangeably (generally) as “ π -mers” or precursor complexes (the designation “dimer” is reserved for the dicationic (D_2)²⁺ complexes²³).

(22) For the spectral and structural characterization of such cation radical “ π -mers”, see: (a) Le Magueres, P.; Lindeman, S.; Kochi, J. K. *J. Chem. Soc., Perkin Trans 2*, **2001**, 1180. (b) Kochi, J. K.; Rathore, R.; Le Magueres, P. *J. Org. Chem.* **2000**, *65*, 6826 and references therein. (c) Charge resonance as employed here derives from Badger, Brocklehurst et al.^{21d–g} to describe the NIR absorption bands associated with the transient cationic dimers of various aromatic donors.

(23) For the formation of the cation radical dimer (PH)₂²⁺ at low temperature, see Figure S6.

(24) Benesi, H. A.; Hildebrand, J. H. *J. Am. Chem. Soc.* **1949**, *71*, 2703.

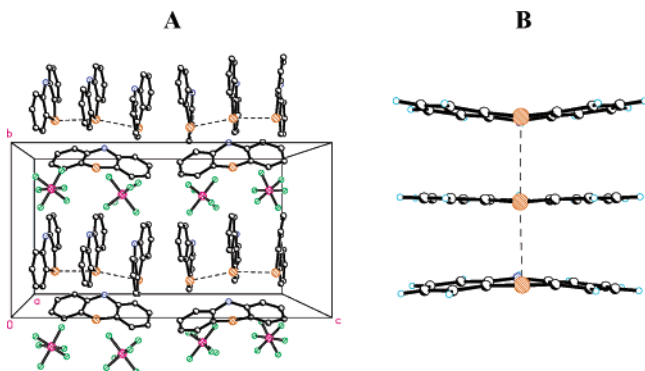


Figure 2. (A) Crystal structure representation of the unit cell of $(\text{PH})_3^{2+}$ - $(\text{PH})(\text{PF}_6)_2$ showing the triplex $(\text{PH})_3^{2+}$ and separate neutral donor. (B) Side view perspective of the triplex $(\text{PH})_3^{2+}$.

coefficient of $\epsilon_{\text{PC}} = 760 \text{ M}^{-1} \text{ cm}^{-1}$ were obtained for eq 2 from the slope and intercept (see Experimental Section). It is noteworthy that the spectral behavior of the *N*-methyl analogue was different, and no new absorption band was observed in the NIR region upon incremental additions of *N*-methylphenothiazine to the solution of PMe^{e+} , even to high molar ratios and at low (down to -80°C) temperatures. We thus concluded that the analogous $(\text{PMe}/\text{PMe}^{e+})$ association was highly limited, and the paramagnetic pimer was too weak to be detected relative to that of the $(\text{PH}/\text{PH}^{e+})$ association under the same conditions.

II. Isolation and X-ray Structure of the Transient Precursor Complex in Intermolecular ET. A. Isolation as a Crystalline [1:1] Complex. Treatment of the pure phenothiazine cation radical salt $\text{PH}^{e+}\text{PF}_6^-$ with 4-fold phenothiazine donor in 1,2-dichloroethane solution showed the diagnostic intervalence band at 1600 nm, the same as that shown in Figure 1. Careful layering of this solution with *n*-hexane and refrigeration at -30°C for 2 weeks afforded well-formed dark brown prisms, with the overall stoichiometric [1:1] composition of $(\text{PH}^+\text{PF}_6^-)(\text{PH})$. Indeed, the solid-state electronic spectrum of this crystalline complex (in KBr pellet) bore a strong resemblance to the corresponding solution spectrum in Figure 1, with the minor exception that the weak intervalence band in the NIR region was slightly red-shifted (Figure S5), consistent with previous comparisons of solid-state and solution spectra.²⁵ In an effort to isolate other crystalline salts of the transient intermolecular complex, we also prepared pure phenothiazine cation radical salts of SbCl_6^- and BF_4^- , but their analogous treatment with free phenothiazine donor merely led to microcrystalline powders unsuitable for X-ray crystallographic analysis.

B. X-ray Crystallography of the [1:1] Complex. The ORTEP diagram of the unit cell in Figure 2 (left) shows that phenothiazine exists in two discrete forms as (a) the molecular triplex dication $(\text{PH})_3^{2+}$ and (b) the uncharged donor PH in the equimolar ratio to constitute the overall [1:1] stoichiometry in the crystalline sample. The bond lengths and angles (Table 2) in the uncharged PH unit are identical to those of the free tub-shaped donor determined independently.²⁶ The stacked triplex shown in Figure 2 (right) consists of cofacial (planar) phenothiazine units separated by a single distance of $d_{\text{D}} = 3.3 \text{ \AA}$, and it

Table 2. Selected Geometric Parameters for the Neutral Phenothiazine Donors and Their Cation Radicals^a

| | a | b | c | d | α^b | β^c | γ |
|---------------------------------|---------|---------|---------|---------|------------|-----------|----------|
| PH^d | 1.763 | 1.391 | 1.367 | 1.399 | 158.5 | | |
| PH^{e+} | 1.708 | 1.399 | 1.368 | 1.379 | 175.7 | | |
| $(\text{PH})_3^{2+}\text{PH}^f$ | 1.737 | 1.399 | 1.385 | 1.377 | 170.1 | | |
| | 1.733 | 1.405 | 1.376 | 1.379 | 177.2 | | |
| | 1.749 | 1.399 | 1.388 | 1.389 | 164.2 | | |
| | 1.771 | 1.384 | 1.397 | 1.396 | 154.4 | | |
| 1 | 1.754 | 1.392 | 1.387 | 1.413 | 154.4 | 87.7 | |
| 1^{*+g} | 1.737 | 1.398 | 1.379 | 1.401 | 171.8 | 90.0 | |
| 2 | 1.762 | 1.391 | 1.387 | 1.413 | 146.6 | 47/87 | 52/11 |
| 2^{*+h} | 1.767 | 1.390 | 1.388 | 1.415 | 140.0 | 48.2 | 54.8 |
| | (1.720) | (1.405) | (1.369) | (1.389) | (165.3) | (84.4) | (8.7) |
| 2^{2+i} | 1.713 | 1.407 | 1.369 | 1.389 | 173.0 | 81/82 | 35/17 |
| 3 | 1.754 | 1.389 | 1.382 | 1.409 | 157.2 | 91.6 | |

^a Bond length in \AA , angles in degrees, average bond lengths are presented if aromatic ring in phenothiazine moieties are nonidentical. For complete characterization, see Table S1 in the Supporting Information. ^b Dihedral angle between the planes of side aromatic rings along the N-S axis. ^c Dihedral angle between the planes of phenothiazine and the bridging aromatic ring. ^d From ref 26a. ^e From ref 26b. ^f Structural data for four independent phenothiazine molecules; see text. ^g As SbF_6^- salt. ^h As $\text{CB}_{11}(\text{CH}_3)_{12}^-$ salt. In parentheses, the second phenothiazine center. ⁱ As SbCl_6^- salt.

is appropriately described as an intermolecular (ternary) π -complex of phenothiazine and two cation radicals (for details, see the Experimental Section). As such, the triplex²⁷ represents a close structural analogue of the paramagnetic pimer²⁸ in intermolecular self-exchange of phenothiazine donor/acceptor dyads as described in eq 2.

III. Intramolecular ET between Bridged (P/P^{e+}) Centers in Mixed-Valence Cation Radicals. A. Synthesis of Bridged Phenothiazine Donors and Their Mononuclear Models. The phenothiazine mixed-valence donor **2** (**2'**) and its mononuclear model **4** (see Table 3) were prepared from the lithium salt of phenothiazine and the corresponding benzyl bromide in THF at room temperature. The bridged donors **1** and **3** as well as their mononuclear model **5** (Table 3) were synthesized by the Ullman coupling of phenothiazine with the corresponding iodobenzene derivatives at 220°C , as described in the Experimental Section.

B. Electrochemical Generation of Mixed-Valence Cation Radicals. Selective (one-electron) oxidations of the various

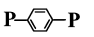
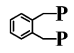
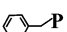
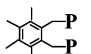
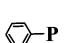
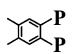
(27) For other comparative studies of 2:1 and 1:1 pimeric structures, see: (a) Le Magueres, P.; Lindeman, S. V.; Kochi, J. K. *Org. Lett.* **2000**, *2*, 3567. (b) We conclude from the bond distance changes and the opening of the dihedral angle α that the effective charge on the central phenothiazine in the triplex is roughly +1.0 and the asymmetric distribution is +0.7 and +0.3 on the terminal phenothiazines (see Table 2, entries 3–5).

(28) (a) Note that the strong similarity of the solid-state spectrum in Figure S5 and the NIR band of the precursor complex in solution (Figure 1) supports such a suggestion. (b) The 3.3 \AA separation is similar to those published previously for different complexes between cation and anion radicals and their neutral precursor (e.g., in the 1:1 pimer of octamethylantracene, which is isoelectronic with phenothiazine).^{26b} The planar moieties within such associates lie atop one another (or somewhat shifted) with the interplanar separation of $3.3 \pm 0.3 \text{ \AA}$ which does not essentially depend on the stoichiometric composition of the particular complex (1:1, 1:2, 2:1, etc.).⁴¹ (c) In the [1:1] charge-transfer complexes between phenothiazine and 7,7,8,8-tetracyanoquinodimethane^{28d} or 1,3,5-trinitrobenzene,^{28c} the donor and acceptor moieties also lie atop each other at the interplanar distance of about 3.4 \AA . (d) Toupet, L.; Carl, N. *Acta Crystallogr., C* **1995**, *51*, 249. (e) Fritchie, C. J., Jr. *J. Chem. Soc. A* **1969**, 1328.

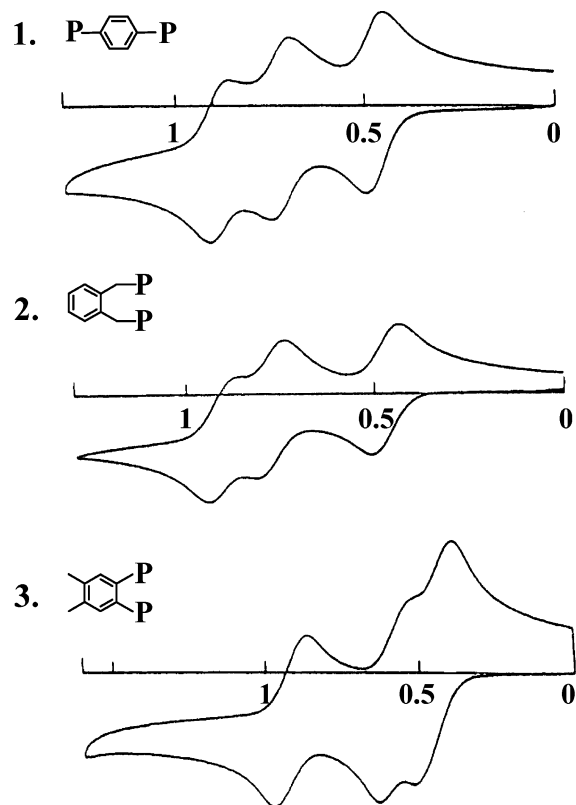
(25) Lü, J.-M.; Rosokha, S. V.; Kochi, J. K. *J. Am. Chem. Soc.* **2003**, *125*, 12161.

(26) (a) McDowell, J. J. H. *Acta Crystallogr., Sect. B* **1976**, *32*, 5. (b) Uchida, T.; Ito, M.; Kozawa, K. *Bull. Chem. Soc. Jpn.* **1983**, *56*, 577.

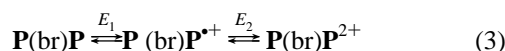
Table 3. Oxidation Potentials of Mixed-Valence and Mononuclear Donors^a

| Mononuclear Donors | E_{ox}^0 (V vs SCE) ^a | Mixed-Valence Donors | E_{ox}^0 (V vs SCE) ^a |
|--|---|---|---|
| PH | 0.61(1e) |  1 | 0.78(1e) 0.92(1e) |
| PMe | 0.79(1e) |  2 | 0.81(1e) 0.98(1e) |
|  4 | 0.79(1e) |  2' | 0.73(1e) 0.90(1e) |
|  5 | 0.74(1e) |  3 | 0.58(1e) 0.92(1e) |

^a From reversible cyclic voltammograms measured at $V = 2 \text{ V s}^{-1}$ in dichloromethane. In parentheses: number of electrons transferred.

**Figure 3.** Initial positive scan cyclic voltammograms of the mixed-valence donors **1**, **2**, and **3** including the ferrocene internal standard at 0.5 V.

phenothiazine donors in Table 3 to the relevant cation radicals were initially examined by cyclic voltammetry. The phenothiazine-containing donors **1**, **2**, and **3** (Figure 3) each showed the initial (one-electron) oxidation to the mixed-valence cation radical followed by a second (well-resolved) oxidation to the dication as described in eq 3, where (br) represents the molecular bridges illustrated in Chart 2, so that the potential



splitting $\Delta E = E_2 - E_1$ represents the energetics of the disproportionation equilibrium ($\Delta G_{\text{disp}} = -RT \ln K_{\text{disp}}$) between the mixed-valence cation radical and the mixed-valence dication.^{29,30} Accordingly, $\Delta E = \Delta G_{\text{disp}}/F$ is a thermodynamic quantity that can be directly related to the stabilization of the electronic interaction between the (P/P^{•+}) redox centers in the

mixed-valence cation radical (relative to the dication plus donor) with $\Delta E = 3.3$, 4.0, and 8.0 kcal/mol for **1**^{•+}, **2**^{•+}, and **3**^{•+}, respectively.³¹ To explore the effects of this electronic interaction on the spectral and structural properties of organic mixed-valence systems, the bridged cation radicals were isolated as crystalline salts (where possible) or prepared in situ (see Experimental Section), and their spectral (UV–vis–NIR/ESR) and structural (X-ray crystallography) properties examined are as follows.

C. Intervalence Transitions in Mixed-Valence Cation Radicals. The electronic spectra of the bridged (mixed-valence) cation radicals **1**^{•+}, **2**^{•+}, and **3**^{•+} were all characterized by the presence of new (low-energy) absorption bands that were singularly absent in the corresponding UV–vis spectra of either (a) the mononuclear (model) cation radicals **4**^{•+} and **5**^{•+} or (b) the bridged dications **1**²⁺, **2**²⁺, and **3**²⁺, as listed in Table 1.

In the *o*-phenylene-bridged cation radical **3**^{•+}, the distinctive low-energy band shown in Figure 4A was cleanly separated from the local bands and red-shifted to the NIR region to closely approximate the intervalence charge-resonance band at 1600 nm of the transient paramagnetic pimer observed in the intermolecular association of phenothiazine with its cation radical as illustrated in Figure 4A (see Experimental Section for details). By comparison, the intervalence absorption band of the *p*-phenylene-bridged cation radical **1**^{•+} was significantly blue-shifted to 910 nm and overlapped the local bands listed in Table 1. However, the digital deconvolution of the vis–NIR envelope via concentration variations (as described in the Experimental Section) revealed the Gaussian-shaped component shown in Figure 4B (inset) and listed in Table 1. Likewise, the intervalence band in the *o*-xylylene-bridged cation radical **2**^{•+} suffered more or less the same blue-shift, and the successful deconvolution of the vis–NIR band envelope revealed the diagnostic absorption band at 943 nm, as described in Figure S6.

D. Intramolecular ET Rates in Mixed-Valence Cation Radicals. The ESR spectrum of the phenothiazine redox center (P^{•+}) was characterized by three major lines corresponding to the principal nitrogen hyperfine splitting further (partially) split by aromatic hydrogens. The values of the hyperfine splitting for the mononuclear models **4**^{•+} and **5**^{•+} identified in Table 4, as well as the ESR line widths, were singularly unchanged in dichloromethane solutions with the variation of temperature. On the other hand, the mixed-valence cation radicals **1**^{•+}, **2**^{•+}, and **3**^{•+} showed two distinctive behavioral patterns as the temperature of the dichloromethane solution was progressively raised from -90 to 30 °C in the following way:

D.1. Temperature-Dependent ESR Line Broadening in Mixed-Valence Cation Radicals **1^{•+} and **2**^{•+}.** Figure 5 (top) shows the well-resolved ESR spectrum at -30 °C of the *p*-phenylene-bridged cation radical **1**^{•+}, which underwent general line broadening upon warming ($+30$ °C) and resulted in the partial obliteration of the hydrogen hyperfine splittings, as illustrated by the computer-simulated spectra in Figure 5 (right).

- (29) (a) Creutz, C. *Prog. Inorg. Chem.* **1983**, *30*, 1. (b) Evans, C. E. B.; Naklicki, M. L.; Rezvani, A. R.; White, C. A.; Kondratiev, V. V.; Crutchley, R. J. *J. Am. Chem. Soc.* **1998**, *120*, 13096.
 (30) (a) Lindeman, S. V.; Rosokha, S. V.; Sun, D.-L.; Kochi, J. K. *J. Am. Chem. Soc.* **2002**, *124*, 843. (b) Rosokha, S. V.; Sun, D.-L.; Kochi, J. K. *J. Phys. Chem. A* **2002**, *106*, 2283.
 (31) See also Table 6, column 7.

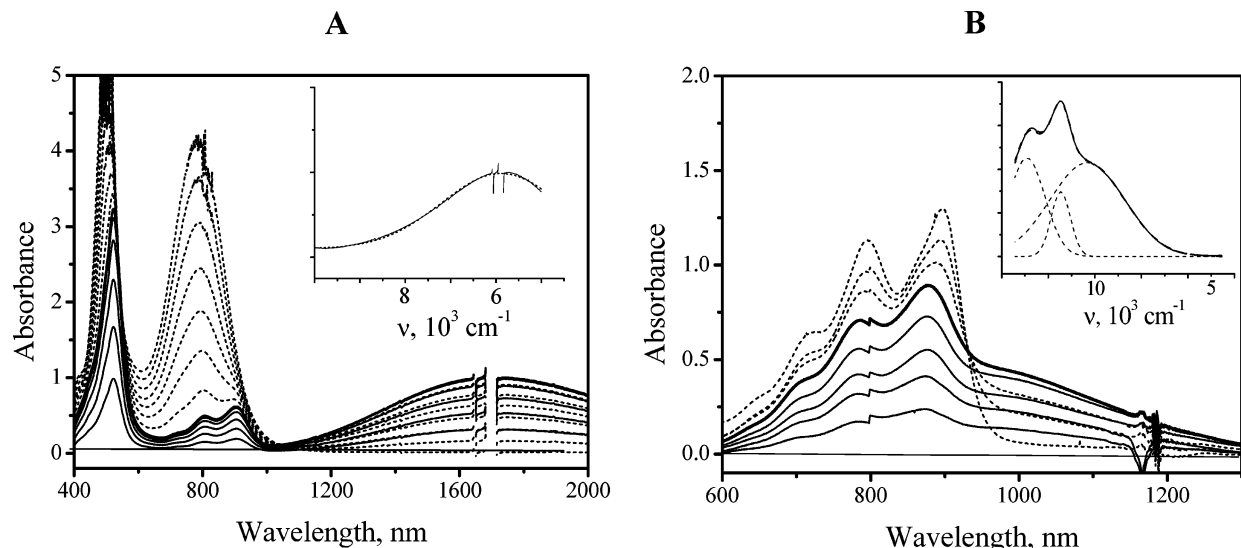


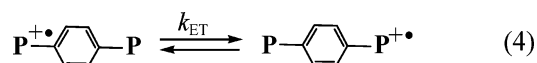
Figure 4. Spectral changes in the NIR region attendant upon the addition of oxidant to the solution of *ortho*-phenylene-bridged phenothiazines **3** (A) and its *para*-phenylene-bridged analogue **1** (B). Concentrations: (A) **3** = 2 mM; oxidant (from bottom to top at 800 nm) 0, 0.4, 0.8, 1.2, 1.6, 2.0, 2.4, 2.8, 3.2, 3.6, 4.0, 4.4, 5.0 mM. (B) **1** = 2 mM, oxidant (from bottom to top at 800 nm) 0, 0.4, 0.8, 1.2, 1.6, 2.0, 2.6, 3.2, 3.8 mM. Note that the low-energy NIR absorption grows until oxidant to **1** (or **3**) ratio is less than 1:1 (solid lines) and decreases when concentration of the oxidant is higher than that of **1** (or **3**) (dashed lines). Insets: Gaussian deconvolution (dashed lines) of the mixed-valence cation radical spectra NIR range (thick, solid lines).

Table 4. ESR Spectral Parameters of the Mixed-Valence Cation Radicals and Their Mononuclear Models

| cation radical | hyperfine splitting constants (G) ^a | | |
|-----------------------|--|----------------------|------------------------------------|
| | N | H ^b | H (aromatic) |
| PH ^{+f} | 6.55(1) | 7.42(1) ^c | 2.59(2), 1.25(2), 0.48(4) |
| PMe ^{+f} | 7.66(1) | 7.31(3) ^d | 2.17(2), 1.02(2), 0.70(2), 0.28(2) |
| 1 ⁺ | 7.04(1) | | 1.41(6), 0.70(2) |
| 2 ⁺ | 7.04(1) | 3.84(2) ^e | 1.99(2), 1.02(4), 0.28(2) |
| 3 ⁺ | 3.52(2) | | 1.00(4), 0.50(8), 0.20(4) |
| 4 ⁺ | 7.04(1) | 3.84(2) ^e | 1.99(2), 1.02(4), 0.28(2) |
| 5 ⁺ | 7.04(1) | | 2.2(2), 0.90(2), 0.35(4) |

^a In parentheses: number of splitting nuclei. ^b As indicated in footnotes c–e. ^c H_N. ^d H_{CH₃}. ^e H_{CH₂}. ^f From ref 18.

Figure 5 also includes the first-order rate constants (k_{ET}) for intramolecular electron exchange in eq 4 of the mixed-valence cation radical **1**⁺ that is typically obtained from the fit of the experimental ESR spectrum to that calculated with the aid of the ESR-EXN program.³²



Similarly, the ESR spectrum of the *ortho*-xylylene-bridged cation radical **2**⁺ (see Chart 2) was readily simulated at low temperature with essentially the same hyperfine splittings pertinent to the ESR spectrum of its mononuclear model **4**⁺ (Table 4 and Figure S7), but upon warming only the ESR spectrum of the mixed-valence cation radical **2**⁺ showed noticeable linebroadening (Figure S8). The latter was assigned

(32) (a) Heinzer, J. *Quantum Chemistry Program Exchange* 209, as modified by Petillo, P. A. and Ismagilov, R. F. We thank Prof. S. F. Nelsen for providing us with a copy of this program. (b) The limited line broadening and rather small changes in k_{ET} over the 120° temperature range in dichloromethane in Figure 5 was not substantially changed in 1,2-dichloroethane at its higher temperature limit ($k_{ET} = 4 \times 10^9 \text{ s}^{-1}$ at +60 °C). Thus, we were unable to attain the requisite temperatures (and enhanced rates of $k_{ET} \approx 1 \times 10^8 \text{ s}^{-1}$) at which the diagnostic alternating line width effects would be observed in the dynamic simulation of the ESR spectra, as we previously showed in a related mixed-valence system.³⁶ We thank a reviewer for pointing out the desirability for such an experimental verification.

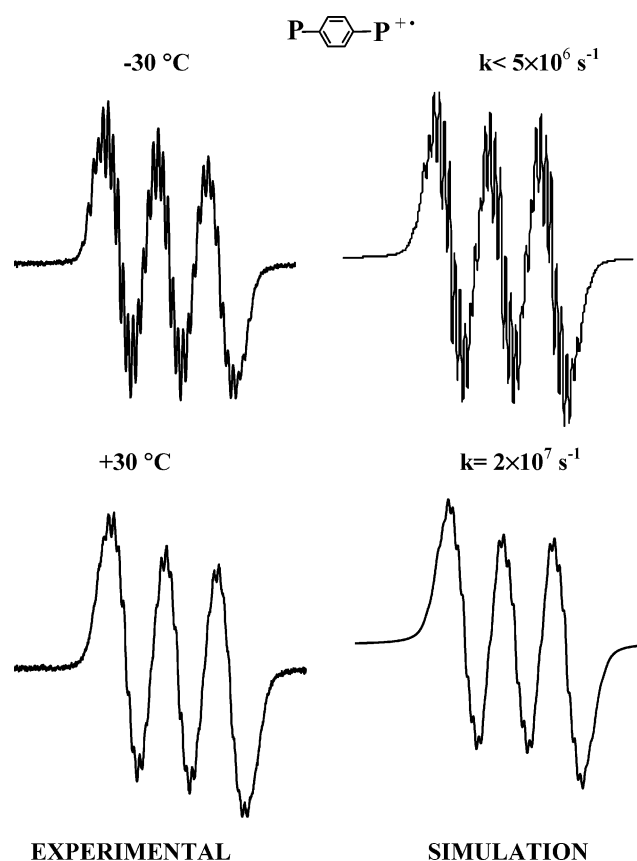
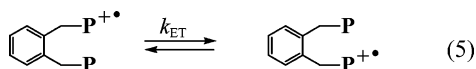
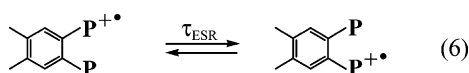


Figure 5. Temperature-dependent ESR line broadening of the mixed-valence cation radical **1**⁺ (left) in comparison with the computer-simulated spectra (right) based on first-order electron exchange.

to dynamic electron exchange, and the fits of the experimental spectra with those calculated with the aid of the ESR-EXN program³² afforded the first-order rate constants for intramolecular ET in eq 5 as $k_{ET} = 2 \times 10^7 \text{ s}^{-1}$ at +30 °C and $k_{ET} \leq 2 \times 10^6 \text{ s}^{-1}$ at -60 °C.



D.2. Temperature-Independent but “Doubled” ESR Spectrum of $3^{+\bullet}$. The ESR spectrum of *ortho*-phenylene-bridged cation radical $3^{+\bullet}$ consisted of five major lines (Figure 6, left), corresponding to hyperfine splitting by 2 equiv nitrogen nuclei, but otherwise with no resolved proton splittings. Computer simulation shown in Figure 6 (right) verified the spectral assignment derived from twice the number of nitrogen splittings with roughly half the coupling constants relative to those found in the mononuclear model $5^{+\bullet}$ and in the mixed-valence cation radical $1^{+\bullet}$ and $2^{+\bullet}$ (Table 4). Such an increased number and decreased splittings of hyperfine lines were characteristic of other dimer cation radicals in which either the unpaired electron is completely delocalized over both redox centers or electron exchange in eq 6 is too fast to be resolved on the ESR time scale with half-life $\tau_{\text{ESR}} < 10^{-9}$ s,³³ i.e.,



Moreover, the latter must be immeasurably fast even at -80 °C since the ESR spectrum was singularly unchanged as the solution was allowed to warm incrementally over a 110° range to ambient temperature.

D.3. Comparative ESR Behavior of Mixed-Valence Dications. The bridged-dependent intermolecular interaction between phenothiazinyl redox centers was also shown in the ESR characteristics of the mixed-valence dication radicals 1^{2+} , 2^{2+} , and 3^{2+} . Thus, the ESR parameters for the *p*-phenylene- and *o*-xylylene-bridged dication radicals (Figure S11) were essentially the same as those in the corresponding mixed-valence cation radicals $1^{+\bullet}$ and $2^{+\bullet}$, to reveal 1^{2+} and 2^{2+} as de facto dication diradicals with (more or less) weakly interacting ($P^{\bullet+}/P$) centers.³⁴ By strong contrast, the *o*-phenylene-bridged dication 3^{2+} was ESR silent, to reveal 3^{2+} as a diamagnetic dication²⁵ with strongly spin-coupled ($P^{\bullet+}/P^{\bullet+}$) centers reminiscent of the strong electronic interaction between ($P/P^{\bullet+}$) centers necessary to describe the ultrafast electron exchange in $3^{+\bullet}$ (eq 6).

IV. Structure Analysis of Mixed-Valence Donors and Cation Radicals. A. X-ray Structure Analyses of *para*-Phenylene-Bridged Systems. The ORTEP diagram of the mixed-valence donor **1** in Figure 7A shows the two (tub-shaped) *para*-phenothiazinyl substituents to be arranged mutually perpendicular to the plane of the connecting phenylene bridge so that 1,4-substitution leads to nearly coplanar phenothiazine redox centers. Upon one-electron oxidation, the mixed-valence cation radical $1^{+\bullet}$ retains the same overall conformation, as shown in Figure 7B. In the neutral donor, the phenothiazine redox centers are both folded along the S–N axis with the dihedral angle of $\theta = 154^\circ$, which is the same as that found in the free phenothiazine donor itself. Oxidation to the cation radical $1^{+\bullet}$ results in the significant planarization of both phenothiazine

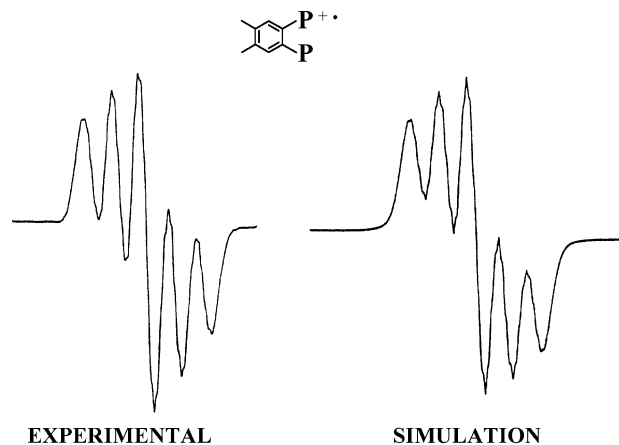
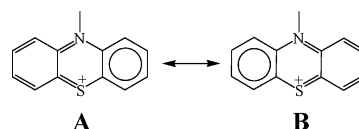


Figure 6. Comparison of the experimental (left) and computer-simulated (right) ESR spectra of the mixed-valence cation radical $3^{+\bullet}$ of the *ortho*-phenylene-bridged donor.

redox centers to $\theta = 172^\circ$, which is the same as that in $PH^{+\bullet}$. There are also significant changes in the N–C, S–C, and C–C bond lengths accompanying the oxidation of the mixed-valence donor **1** to its cation radical (Table 2) to suggest a significant contribution from resonance structures A and B pertinent to the pair of partially oxidized phenothiazine moieties shown below.³⁵



Furthermore, it is important to note that both the mixed-valence donor **1** as well as its cation radical $1^{+\bullet}$ possess crystallographic centers of symmetry so that the redox centers (P/P) and ($P/P^{\bullet+}$) are pairwise equivalent. In particular, the results in Table 2 are consistent with partial (positive) charge that is equally distributed between both phenothiazine redox centers in the mixed-valence cation radical $1^{+\bullet}$, in accord with the dynamic equilibrium in eq 3.^{35a}

B. Structures of *o*-Xylylene-Bridged Mixed-Valence Systems. Mixed-valence systems such as **2** that incorporate the *ortho*-xylylene bridge are conformationally flexible³⁶ and often not readily crystallized. Nonetheless, we were able to examine the parent donor **2**, its cation radical $2^{+\bullet}$, and its dication 2^{2+} as single crystals suitable for X-ray. The structures of **2**, $2^{+\bullet}$, and 2^{2+} show the same trend in bond length and angle changes as those described for the *p*-phenylene-bridged analogues in Table 2. The ORTEP diagram of the mixed-valence donor **2** in Figure 8A presents the conformation with partial overlap of the two (tub-shaped) phenothiazine redox centers (resulting from different rotations about the pair of methylene bonds; Table 2) and center-to-center separation of $d_D \approx 5.2$ Å. One-electron oxidation to the mixed-valence cation radical results in the planarization of only one phenothiazine center (the other maintaining its tub shape), but otherwise, $2^{+\bullet}$ retains the overall conformation of parent donor, as shown in Figure 8B. Two-

(33) (a) Gerson, F.; Kaupp, G.; Ohya-Nishiguchi, H. *Angew. Chem., Int. Ed. Engl.* **1977**, *16*, 657. (b) Wartin, A. R.; Valenzuela, J.; Staab, H. A.; Neugebauer, F. A. *Eur. J. Org. Chem.* **1998**, *139*, 9. (c) Lau, W.; Kochi, J. K. *J. Org. Chem.* **1986**, *51*, 1801.

(34) (a) This conclusion accords with that of Okada et al.^{34b} who described 1^{2+} as a triplet (ground-state) dication diradical (or as a nearly degenerate singlet/triplet ground state).^{34b} (b) Okada, K.; Imakura, T.; Oda, M.; Murai, H. *J. Am. Chem. Soc.* **1996**, *118*, 3047.

(35) (a) The equivalency of two phenothiazines in the X-ray structure of $1^{+\bullet}$ may also result from the crystallographic disorder of $P^{\bullet+}/P$ redox centers. (b) For a discussion of this crystallographic point as it applies to a related aromatic redox center, see Le Magueres, P. et al. in ref 22a and Lindeman et al. in ref 30a.

(36) Sun, D.-L.; Rosokha, S. V.; Lindeman, S. V.; Kochi, J. K. *J. Am. Chem. Soc.* **2003**, *125*, 15950.

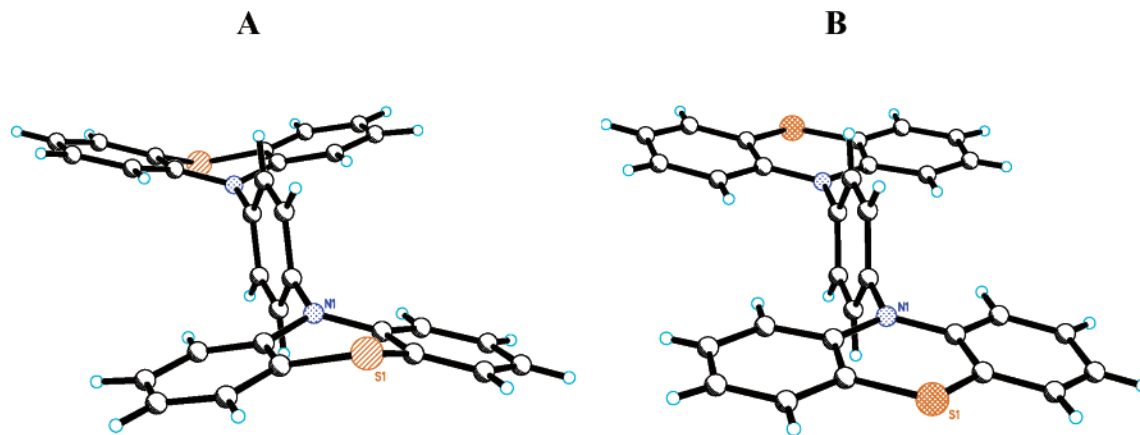


Figure 7. Molecular structures of the *para*-phenylene-bridged mixed-valence donor (A) and its cation radical (B) showing the same pair of tub/tub-shaped phenothiazine redox centers in **1**, but planar/planar in **1**^{•+} (as SbCl₆⁻ salt).

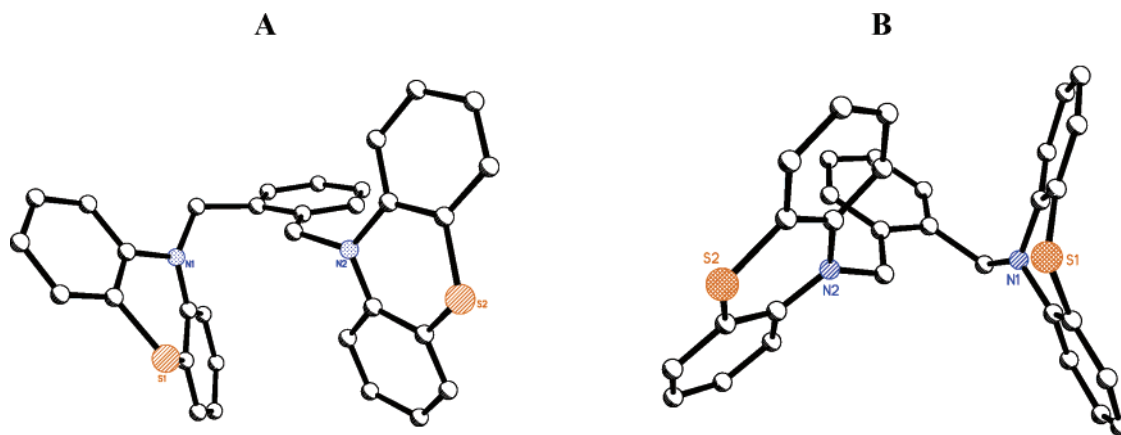


Figure 8. Equivalent conformations of the *ortho*-xylylene-bridged mixed-valence donor (A) and its corresponding cation radical (B) showing roughly the same cofacial disposition of the phenothiazine redox centers which are both tub/tub-shaped in **2**, but planar/tub in **2**^{•+} (as CB₁₁(CH₃)₁₂⁻ salt).

electron oxidation to the dication **2**²⁺ is accompanied by a sizable rotational change to a more trans-like conformation (Figure S12) with two (planar) phenothiazines more or less coplanar in the manner reminiscent of that in the *p*-phenylene analogue **1** established in Figure 7A. The changes in the internal geometries of the phenothiazinyl centers accompanying two-electron oxidation to **2**²⁺ were similar to those in Table 2 for the *p*-phenylene-bridged pair (vide supra). Such structural changes indicate that the dication **2**²⁺ consists of a pair of discrete (equivalent) phenothiazinyl redox centers that are rather weakly interacting in accord with the ESR analysis (vide supra).

C. X-ray Structure of the *o*-Phenylene-Bridged Donor. The structurally rigid mixed-valence donor **3** was obtained as a single crystal, and the ORTEP diagram (Figure S9) identifies the pairs of cofacial phenothiazine centers separated by a (center-to-center) distance of $d_D = 3.3 \text{ \AA}$ (Table 2) that slightly deviates from a parallel arrangement by a dihedral angle of $\theta = 40^\circ$. Although we were able to isolate both the mixed-valence cation radical **3**^{•+} and the dication **3**²⁺ as microcrystalline powders, we were unable to grow single crystals suitable for X-ray crystallographic analysis.

Discussion

Intermolecular ET is observed as overall second-order kinetics of freely diffusing electron donors and acceptors, which in the case of the simple self-exchange process pertinent to this study

are represented by phenothiazine (PH) and phenothiazine cation radical (PH^{•+}), respectively. The corresponding first-order process (to obviate diffusion) is then represented in this study by mixed-valence systems **P**(br)**P**^{•+} in which a pair of phenothiazine redox centers are interlinked by the variety of molecular bridges (br) illustrated in Chart 2. We now find that the direct mechanistic interrelationship between intermolecular and intramolecular ET is made via diagnostic transient (optical) changes, as follows.

I. Common Observation of Intervalence Absorptions in Both Intermolecular and Intramolecular ET. The consistent appearance of the new (unique) absorption band in various (PH/PH^{•+}) mixtures in Figure 1 arises from the intervalence transition in the transient [1:1] complex or “pimer” that is spontaneously formed by the intermolecular association according to eq 2. Such a near-IR band has been previously associated with charge-resonance transition of cofacially oriented aromatic donor/acceptor dyads^{21,22} which are structurally represented in this phenothiazine study by the ORTEP diagram in Figure 2.

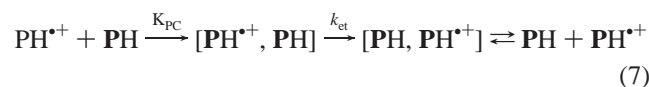
The interconnection of phenothiazine (P/P^{•+}) redox centers represented by mixed-valence cation radicals **1**^{•+}, **2**^{•+}, and **3**^{•+} in Table 1 also results in diagnostic near-IR absorption bands that strongly depend on the nature of the molecular bridge. To relate these intramolecular intervalence absorption bands with the charge-resonance absorption of the intermolecular (pimer) intermediate, let us first describe how the latter plays a critical kinetics role in the mechanism of intermolecular ET.

Table 5. Comparison of Experimental (from ESR data) and Calculated Intramolecular Electron-Transfer Rate Constant in Mixed-Valence Cation Radicals and Intermolecular Self-Exchange

| MVCR | λ , kcal/mol | ΔG^* , kcal/mol | | k_{ET} (+30 °C), s ⁻¹ | |
|---------------------------------|----------------------|-------------------------|--------------------|------------------------------------|-------------------------|
| | | theor ^a | exptl ^c | theor ^b | exptl ^d |
| (PH) ₂ ²⁺ | 17 | 2.5 | 2.6 | 1.2 × 10 ^{10e} | 0.5 × 10 ^{10f} |
| 1 ^{•+} | 30 | 6.4 | 7.2 | 3 × 10 ⁷ | 2 × 10 ⁷ |
| 2 ^{•+} | 31 | 6.3 | 7.2 | 3 × 10 ⁷ | 2 × 10 ⁷ |
| 3 ^{•+} | 16 | 1.2 | | 1.3 × 10 ¹¹ | > 10 ⁹ |

^a From $\Delta G^* = (\lambda - 2H_{IV})^2/(4\lambda)$ based on $\lambda = \nu_{IV}$ and H_{IV} from Table 6. ^b From $k_{ET} = 10^{12} \exp(-\Delta G^*/RT)$, unless otherwise noted. ^c Estimated from temperature dependence of experimental rate constant, ± 2 kcal/mol. ^d From ESR line broadening. ^e Diffusion-corrected second-order rate constant of self-exchange k_{se} calculated from $1/k_{se} = 1/k_{diff} + 1/(K_{PC}k_{ET})$ at 25 °C. ^f Second-order rate constant of self-exchange evaluated from concentration-dependent ESR line broadening at 25 °C.

II. The Mechanism of Intermolecular ET via the Precursor Complex of Phenothiazine Redox Dyads. The generalized (self-exchange) kinetics between an aromatic donor and its cation radical must include the generic precursor complex,^{2,37} and such an ET mechanism for phenothiazine oxidation–reduction is represented by:



where K_{PC} is the intermolecular association constant of the precursor complex and k_{et} is the first-order exchange rate within the precursor complex, herein described as the pimer. The independent evaluations of the association constant as $K_{PC} = 5 \text{ M}^{-1}$ (see eq 2), together with the first-order rate constant theoretically evaluated from the intervalence band as $k_{et} = 1.4 \times 10^{10} \text{ s}^{-1}$ (vide infra), lead to the second-order rate constant for intermolecular ET as $k_{SE}(\text{theor}) = 1.2 \times 10^{10} \text{ M}^{-1} \text{ s}^{-1}$.³⁸ The corresponding experimental second-order rate constant $k_{SE}(\text{exptl})$ obtained directly from the ESR line broadening experiments is also included in Table 5 (column 6). It is thus noteworthy that the theoretical prediction (column 5) based on the generalized mechanism for intermolecular ET according to eq 7 is within acceptable limits of the experimental results.

III. Electronic Coupling in the Precursor Complex (Pimer). The transient character of the precursor complex in intermolecular ET largely precludes a direct (structural) examination of the electronic coupling element H_{DA} that is required for quantitative evaluation of the activation barrier according to eq 1. Thus, let us now turn to the charge-resonance absorption band at 1600 nm that is observed in the intermolecular pimer (Figure 1) and simply relate it to the analogous absorptions in mixed-valence systems (Figure 4). Using the Mulliken formalism,³⁹ Hush showed that the electronic coupling element (H_{DA}) between redox centers in mixed-valence complexes can be estimated directly from the intervalence absorption bands as:⁴⁰

$$H_{IV} = 0.0206(\nu_{\max} \Delta\nu_{1/2} \epsilon)^{1/2} / r_{DA} \quad (8)$$

where ν_{\max} and $\Delta\nu_{1/2}$ are the maximum and full-width at half-

(37) Ganesan, V.; Rosokha, S. V.; Kochi, J. K. *J. Am. Chem. Soc.* **2003**, *125*, 2559.

(38) For the detailed description of intermolecular ET kinetics, see the following discussion.

(39) (a) Mulliken, R. S. *J. Am. Chem. Soc.* **1952**, *74*, 811. (b) Mulliken, R. S. *J. Phys. Chem.* **1952**, *56*, 801. (c) Mulliken, R. S.; Person, W. B. *Molecular Complexes*; Wiley: New York, 1969.

Table 6. Estimation of the Electronic Coupling Elements in Organic (Mixed-Valence) Cation Radicals and Cation Radical Pimer via Mulliken–Hush Formalism (from the Intervalence Band) and Cyclic Voltammetry Data

| MVCR | r_{DA} ^a | ν_{IV} | $\Delta\nu_{IV}$ ^b | ϵ | H_{IV} ^b | ΔE | H_{IP} ^c |
|---------------------------------|-----------------------|----------------------------------|----------------------------------|--|----------------------------------|------------|----------------------------------|
| | Å | 10 ³ cm ⁻¹ | 10 ³ cm ⁻¹ | 10 ³ M ⁻¹ cm ⁻¹ | 10 ³ cm ⁻¹ | V | 10 ³ cm ⁻¹ |
| (PH) ₂ ²⁺ | 3.3 | 5.8 | 2.5 | 0.76 | 0.66 | | |
| 1 ^{•+} | 8.6 | 10.3 | 3.2 | 0.86 | 0.40 | 0.17 | 2.66 |
| 2 ^{•+} | 5.2 | 10.6 | 4.8 | 0.36 | 0.53 | 0.14 | 2.45 |
| 3 ^{•+} | 3.3 | 5.6 | 3.0 | 2.5 | 1.28 | 0.34 | 2.77 |

^a Separation between the centers of phenothiazinyl moieties. ^b Bandwidth at half-height. ^c Calculated with Mulliken–Hush expression (eq 8). ^d Calculated from $F\Delta E = \Delta G_{disp} = 2H^2/\lambda$

heights, respectively (in cm⁻¹), of the absorption band, ϵ is the molar extinction coefficient at the absorption maximum (in M⁻¹ cm⁻¹), and r_{DA} is the effective ET distance (in Å). An important point in such an analysis of the phenothiazine redox dyad is the proper choice of the separation parameter r_{DA} , in other words, the structural characterization of the intermolecular pimer (PH)₂²⁺ in eq 2. In the absence of the X-ray structure of the [1:1] precursor complex, we based our analysis on the triplex shown in Figure 2 as the isolable close relative since it is the crystallizable (equimolar) form out of solution. Although the triplex includes a single neutral donor with a pair of cation radicals, the initial step in the formation of this [2:1] complex is preceded by a prior [1:1] association, and we take half of the triplex to be a reasonable approximation for $r_{DA} = 3.3 \text{ Å}$ as the cofacial separation of (P/P^{•+}) redox centers in the precursor complex.^{28,41}

Utilization of eq 8 with the spectral characteristics of the near-IR absorption band in Figure 1 and the separation distance of $r_{DA} = 3.3 \text{ Å}$ leads to the value of $H_{DA} = 6.6 \times 10^2 \text{ cm}^{-1}$ for the electronic coupling element within the precursor complex for the (PH/PH^{•+}) self-exchange (Table 6).⁴²

IV. Evaluation of the Electronic Coupling Element in Mixed-Valence Systems. A. The *para*-Phenylene-Bridged Cation Radical 1^{•+}. The application of the Mulliken–Hush formalism (eq 8) to the mixed-valence system 1^{•+} in Table 6 follows from the earlier studies of Nelsen, Lambert, and co-workers^{43,44} who employed the same structurally rigid *para*-

(40) (a) Hush, N. S. *Z. Electrochem.* **1957**, *61*, 734. (b) Hush, N. S. *Trans. Faraday Soc.* **1961**, *57*, 557. (c) Hush, N. S. *Prog. Inorg. Chem.* **1967**, *8*, 391. (d) Hush, N. S. *Electrochim. Acta* **1968**, *13*, 1005.

(41) (a) Note that previous studies showed that the separation d_D in [2:1] complexes is close to that in the corresponding [1:1] associations.^{41c,d} (b) Strictly speaking, in extended (organic) redox systems, the separation parameter in eq 8 is difficult to evaluate precisely for two principal reasons: (i) the “distance” refers to the separation between two hypothetical (diabatic) states^{3a,41e} and (ii) the “charge” is highly diffuse. In this study, we utilize the experimentally accessible X-ray structures to approximate the distance between centroids, which in the case of phenothiazines is arbitrarily chosen to lie between N/S atoms. In an ongoing collaboration with M. D. Newton, preliminary results indicate that the calculated values of r_{DA} in the pimer (PH)₂²⁺ is close to that based on X-ray studies. (c) Hanson, A. W. *Acta Crystallogr.* **1968**, *B24*, 773. (d) Fritchie, C. J.; Arthur, P., Jr. *Acta Crystallogr.* **1966**, *21*, 139. (e) See also: Nelsen, S. F.; Newton, M. D. *J. Phys. Chem.* **2000**, *104*, 10023.

(42) The two-state model for ET is based on orthogonal initial and final diabatic states. The extent to which there is orbital overlap between cofacial redox centers violates this restriction, but only strictly speaking. What is not yet known is the degree to which even a modicum of orbital overlap completely violates the applicability of the two-state model, and it thus remains to be seen (by further studies such as this) as to how far this restriction can be further tested with other (orbital) combinations.

(43) (a) Nelsen, S. F.; Adamus, J.; Wolff, J. J. *J. Am. Chem. Soc.* **1994**, *116*, 1589. (b) Nelsen, S. F.; Trieber, D. A.; Wolff, J. J.; Powell, D. R.; Rogers-Crowley, S. J. *J. Am. Chem. Soc.* **1997**, *119*, 6873. (c) Nelsen, S. F.; Ramm, M. T.; Wolff, J. J.; Powell, D. R. *J. Am. Chem. Soc.* **1997**, *119*, 6863. (d) Nelsen, S. F.; Ismagilov, R. F.; Powell, D. R. *J. Am. Chem. Soc.* **1997**, *119*, 10213.

phenylene bridge in various mixed-valence cation radicals with redox centers derived from different N-centered donors, and our later study of intramolecular electron exchange between benzenoid redox centers mirrored the earlier results.^{30,36} Such impressive agreements thus serve as the first step in a test of the Mulliken–Hush two-state model to correctly predict the electronic coupling element in the mixed-valence cation radical $\mathbf{1}^{\bullet+}$ containing a pair of (more or less) planar phenothiazine redox centers. As such, the characteristics of the NIR absorption band in Table 1 (third entry), together with the separation parameter of $r_{\text{DA}} = 8.6 \text{ \AA}$ obtained from X-ray crystallographic data, leads to the value of $\mathbf{H}_{\text{DA}} = 4.0 \times 10^2 \text{ cm}^{-1}$ from eq 8 based on the assignment of the *p*-phenylene-bridged cation radical $\mathbf{1}^{\bullet+}$ to the Class II category of Robin–Day mixed-valence systems.^{45,46} The latter classification also allows the reorganization energy (λ) to be directly evaluated from the intervalence absorption band, i.e., $\nu_{\text{IV}} = \lambda$, as listed in Table 6 (third column).

B. The *ortho*-Xylylene-Bridged Cation Radical $\mathbf{2}^{\bullet+}$. The conformationally flexible mixed-valence cation radical $\mathbf{2}^{\bullet+}$ has the potential to juxtapose the pair of ($\mathbf{P}/\mathbf{P}^{\bullet+}$) redox centers in the cofacial arrangement akin to that extant in the intermolecular pimer shown in Figure 2.⁴⁷ However, the extended and distinctly nonplanar phenothiazine at one redox center is apparently too large to accommodate such an intimate (face-to-face) arrangement of both ($\mathbf{P}/\mathbf{P}^{\bullet+}$) redox centers, and a compromise is struck in the stable conformational structure shown in Figure 8B, in which a separation distance of $r_{\text{DA}} = 5.2 \text{ \AA}$ is evaluated.⁴⁸ This, together with the analogous application of Mulliken–Hush formalism in eq 7 to the intervalence absorption band of $\mathbf{2}^{\bullet+}$ in Table 1 (fifth entry), leads to $\mathbf{H}_{\text{DA}} = 5.3 \times 10^2 \text{ cm}^{-1}$ for electronic coupling element and the reorganization energy of $\lambda = 10.6 \times 10^3 \text{ cm}^{-1}$.

C. The *ortho*-Phenylene-Bridged Cation Radical $\mathbf{3}^{\bullet+}$. The direct attachment of the redox centers to an *o*-phenylene bridge as in the structurally rigid mixed-valence cation radical $\mathbf{3}^{\bullet+}$ juxtaposes the ($\mathbf{P}/\mathbf{P}^{\bullet+}$) centers at a separation distance of $r_{\text{DA}} = 3.3 \text{ \AA}$ (with a tilt of $\theta = 40^\circ$).⁴⁹ Together with the highly red-shifted intervalence absorption band to 1700 nm (Table 1), the application of Hush eq 8⁵⁰ leads to $\mathbf{H}_{\text{DA}} = 1.28 \times 10^3 \text{ cm}^{-1}$ for the electronic coupling element and the reorganization energy of $\lambda = 5.6 \times 10^3 \text{ cm}^{-1}$ that is surprisingly close to that of the intermolecular pimer (see Table 5 column 2).

D. Alternative (Thermodynamics) Estimation of the Electronic Coupling Element. The electronic interaction between a pair of redox centers in a mixed-valence systems can be alternatively estimated by an electrochemical method. Thus, the

electronic interaction between ($\mathbf{P}/\mathbf{P}^{\bullet+}$) redox centers results in the resonance stabilization of the mixed-valence state that is inherent to the driving force for the disproportionation equilibrium,²⁹ e.g.: the free-energy change of which is given by ΔG_{disp}



$= F\Delta E_{1/2}$, where $\Delta E_{1/2} = E_{1/2}(2) - E_{1/2}(1)$ as described in eq 3. Although the free energy of disproportionation ΔG_{disp} is determined as the sum of several factors, the contribution from the resonance stabilization of the mixed-valence cation radical is generally the major component.⁵¹ As such, the electronic coupling element can be evaluated thermodynamically from the reversible oxidation data as⁸ $\mathbf{H}_{\text{TD}} = (\lambda\Delta G_{\text{disp}}/2)^{1/2}$, and the values of the electronic coupling element obtained from the cyclic voltammetric measurements in Figure 3 are listed in Table 6 (column 8) for the mixed-valence cation radicals $\mathbf{1}^{\bullet+}$, $\mathbf{2}^{\bullet+}$, and $\mathbf{3}^{\bullet+}$. Although such a thermodynamics analysis represents the upper limit to the effective electronic coupling element,^{51,52} the significant discrepancies between the CV-based values of \mathbf{H}_{TD} (column 8) and the spectral-based values of \mathbf{H}_{IV} (column 6) raise a question as to the applicability of the Mulliken–Hush (two-state) formalism to reliably predict the electronic coupling element from the intervalence absorption bands in mixed-valence cation radicals ($\mathbf{1}^{\bullet+}$, $\mathbf{2}^{\bullet+}$, and $\mathbf{3}^{\bullet+}$) and in the intermolecular pimer (\mathbf{PH}_2)⁵³. Accordingly, we now turn to the earlier approach of Newton, Nelsen, and co-workers,⁵⁴ who addressed this fundamental problem by the direct comparison of the predicted rates of intermolecular ET based on \mathbf{H}_{IV} from the Mulliken–Hush treatment with the experimental rates obtained independently, as follows.

V. Testing the Two-State Model for Intramolecular and Intermolecular ET between Phenothiazine Redox Centers.

A. Intramolecular ET in Mixed-Valence Cation Radicals. The intramolecular rate constant can be evaluated within the Marcus–Hush formalism as:²

$$k_{\text{ET}} = \kappa \nu_n \exp(-\Delta G^*/RT) \quad (10)$$

where κ is the electronic transmission coefficient, ν_n is the nuclear vibration frequency related to ET, and ΔG^* is the activation free energy for ET. When the electronic coupling is

- (44) (a) Lambert, C.; Noll, G. *J. Am. Chem. Soc.* **1999**, *121*, 8434. (b) Holzapfel, M.; Lambert, C.; Selinka, C.; Stalke, D. *J. Chem. Soc., Perkin Trans. 2* **2002**, 1553.
- (45) The value of r_{DA} as estimated from molecular structure of $\mathbf{1}^{\bullet+}$ is very close to the distance between the spin centers in dication diradical $\mathbf{1}^{2+}$ as determined by Okada et al.^{34b} from its ESR (triplet) spectrum.
- (46) (a) The mixed-valence cation radical $\mathbf{1}^{\bullet+}$ is assigned to the Robin–Day Class II category^{46b} based on the ESR characteristics showing electron localization of the unpaired electron on a single phenothiazine redox center, and the same applies to the *o*-xylylene-bridged cation radical $\mathbf{2}^{\bullet+}$. Furthermore, the values of $\mathbf{H}_{\text{AD}} < \lambda/2$ in Table 6 support the assignment of these systems to Class II. (b) Robin, M. B.; Day, P. *Adv. Inorg. Chem. Radiochem.* **1967**, *10*, 247.
- (47) For such a syn conformation in the analogous *o*-xylylene-bridged cation radical with benzenoid redox centers, see Sun, D.-L. et al. in ref 36.
- (48) It is important to note that the configuration of the two phenothiazine centers in $\mathbf{2}$, $\mathbf{2}^{\bullet+}$, and $\mathbf{2}^{2+}$ systematically change from tub/tub, tub/planar, and planar/planar, respectively. See text for the mechanistic implications of such structural changes in the phenothiazine redox centers.
- (49) Compare with the ORTEP structure in Figure S10.

- (50) (a) Although $\mathbf{3}^{\bullet+}$ may appear to be delocalized on the ESR time scale of $\tau \approx 10^{-9}$ s, we tentatively conclude that it falls into the Robin–Day Class II category based on the solvent dependence of the intervalence band as seen by the blue-shift with increasing solvent polarity as described in Table S1. (b) A reviewer has suggested that the intervalence bandwidth of $\mathbf{3}^{\bullet+}$ ($\Delta\nu_{1/2} = 3.0 \times 10^3 \text{ cm}^{-1}$) is less than the theoretically predicted values for Class II,⁴⁰ i.e., $\Delta\nu_{1/2} = (2300\nu_{\text{IV}})^{1/2} = 3600 \text{ cm}^{-1}$. However, a discrepancy of 600 cm^{-1} is not uncommon (see: Elliot et al. in ref 54). (c) Even if this were so, our basic conclusions would remain unchanged since the electronic coupling element for Class III would be roughly twice as large (i.e., $\mathbf{H}_{\text{IV}} = h\nu_{\text{IV}}/2 = 2.8 \times 10^3 \text{ cm}^{-1}$), and the reorganization energy would be less (not greater) than the maximum values listed in Tables 5 and 6.
- (51) Note that \mathbf{H}_{TD} evaluated from the electrochemical data is expected to represent an upper limit to the intrinsic electronic coupling element because of the neglect of the other energy terms.^{36,52}
- (52) A reviewer has also indicated that the correlation between ΔG_{disp} and H_{ab} is generally weaker for the organic intervalence compounds with aromatic redox centers (due to small solvation difference between dication and cation) than for the usual mixed-valence coordination compounds.
- (53) Since the MHS (two-state) model requires the diabatic states to be orthogonal,²⁸ the orbital overlap that may exist in pimer (\mathbf{PH}_2)⁵³ and mixed-valence cation radical $\mathbf{2}^{\bullet+}$ and $\mathbf{3}^{\bullet+}$ may necessitate some correction of the parameters obtained via eq 8.
- (54) For previous examples of the application of such a test, see: Elliot, C. M.; Derr, D. L.; Matyushov, D. V.; Newton, M. D. *J. Am. Chem. Soc.* **1998**, *120*, 11714, and Nelsen and co-workers in ref 43.

sufficiently strong, as given in Table 6, κ can be taken as unity (i.e., adiabatic ET), and the activation barrier is given by Marcus–Hush eq 1. The theoretically predicted activation free energies $\Delta G^*(\text{theor})$ evaluated in this manner from the reorganization energy (λ) and the electron coupling element (H_{IV}) in Table 5 show consistently reasonable agreements with the experimental values derived from the temperature dependence of the ET rate constant evaluated by ESR (line broadening) measurements as $\Delta G^*(\text{exptl})$ in column 4. The same reasonable agreement is also observed in Table 5 (columns 5 and 6) between the predicted rate constant $k_{\text{ET}}(\text{theor})$ that is based on $\Delta G^*(\text{theor})$ with $\nu_n = 10^{12} \text{ s}^{-1}$ ⁵⁵ and the experimental rate constant k_{ET} derived from ESR line-broadening measurements for both $1^{+\bullet}$ and $2^{+\bullet}$. We take this convergence to constitute a valid test for the reliable evaluation of the electronic coupling element via the Mulliken–Hush analysis of the intervalence absorption band.⁵⁶ Since the proximal arrangement of $P/P^{+\bullet}$ in the *o*-xylylene-bridged cation radical $2^{+\bullet}$ is reminiscent of that extant in the intermolecular pimer taken in Figure 2, let us also apply the Mulliken–Hush analysis to this transient intermediate as it applies to the precursor complex in intermolecular ET.

B. Intermolecular ET via the Precursor Complex. The direct observation of the charge-resonance (NIR) band in the intermolecular association of the free phenothiazine donor (PH) and its cation radical (PH⁺) in Figure 1 leads (based on Mulliken–Hush analysis) to the electronic coupling element $H_{IV} = 6.6 \times 10^2 \text{ cm}^{-1}$ and the other parameters listed in Table 6 (entry 1) for the pimeric precursor complex (PH)₂⁺. Applying the Marcus–Hush methodology presented in eq 8, we evaluated the intramolecular electron exchange within the precursor complex as $k_{\text{et}} = 1.4 \times 10^{10} \text{ s}^{-1}$. According to the mechanistic pathway in Scheme 1 (eq 7), the theoretically predicted second-order rate constant for phenothiazine self-exchange includes the precursor complex and is given by $k_2 = K_{\text{PC}}k_{\text{et}} = 7 \times 10^{10} \text{ M}^{-1} \text{ s}^{-1}$, when $K_{\text{PC}} = 5 \text{ M}^{-1}$, as evaluated in eq 2. Since this self-exchange is close to the diffusion-controlled limit, explicit correction for diffusion must be taken into account as $k_{\text{SE}}(\text{theor}) = k_2k_{\text{diff}}/(k_2 + k_{\text{diff}}) = 1.2 \times 10^{10} \text{ M}^{-1} \text{ s}^{-1}$, where $k_{\text{diff}} = 1.5 \times 10^{10} \text{ M}^{-1} \text{ s}^{-1}$ in dichloromethane at 25 °C.⁵⁷ This theoretically predicted value of second-order rate constant for the self-exchange is included in Table 5 (column 5) and compares favorably with the experimental rate constant of $k_{\text{SE}}(\text{exptl}) = 0.5 \times 10^{10} \text{ M}^{-1} \text{ s}^{-1}$ in column 6, especially if due cognizance is taken of the uncertainty in our evaluation of the preexponential factor.⁵⁵

To circumvent any ambiguity in ν_n , the theoretical prediction can be alternatively tested by the direct comparison of the activation energies. Thus, the theoretical barrier predicted in eq 1 from the electronic coupling element and the reorganization

energy in Table 5 is $\Delta G_{\text{ET}}^\ddagger = 2.5 \text{ kcal mol}^{-1}$. This value compares quite favorably with the experimentally measured values of the activation barrier $E_a = 2.2 \text{ kcal mol}^{-1}$ obtained from the temperature-dependent ESR line widths.⁵⁸

VI. Electronic Effects of Strong Donor–Acceptor Coupling on Intermolecular and Intramolecular ET. Direct comparison of theoretically predicted and experimental values of activation barriers and ET rates between ($P/P^{+\bullet}$) centers indicates that Marcus–Hush eq 1, together with the two-state Mulliken–Hush eq 8, provides a suitable description of intermolecular and intramolecular ET rates when strong electronic couplings in the intermolecular pimer (PH)₂⁺ and the mixed-valence cation radicals $P(\text{br})P^{+\bullet}$ are taken into account. It is particularly noteworthy that the electronic couplings obtained from the intervalence (optical) transitions in Table 6 thus appear to be meaningful and reasonably accurate for ($P/P^{+\bullet}$) interactions in the intermolecular pimer and in the mixed-valence cation radical. If so, we now inquire as to what kind of mechanistic insight may be gained from an inquiry into the ET parameters listed in Table 6. For example, the values of the electronic coupling element evaluated by the Mulliken–Hush procedure for the intermolecular pimer (PH)₂⁺ is comparable to that in the *o*-xylylene-bridged cation radical $2^{+\bullet}$, but the ET reorganization energy is substantially lower than that for $2^{+\bullet}$. Such a divergence may be related to the somewhat different arrangement of phenothiazine moieties in (PH)₂⁺ in comparison with that presented in Chart 2, and the strong electronic coupling of the cofacial ($P/P^{+\bullet}$) redox centers in the intermolecular pimer (see Figure 2) may arise from incomplete solvation and resultant decrease in the outer-sphere reorganization energy.⁵⁹ By contrast, such a solvent restriction is less unfavorable in the partially overlapped ($P/P^{+\bullet}$) centers in $2^{+\bullet}$, and the larger interplanar separation could result in increased solvation of the mixed-valence cation radical relative to that in the “tight” intermolecular pimer. Such a tentative suggestion is also supported by a comparison of the *p*-phenylene-bridged cation radical $1^{+\bullet}$ and the *o*-phenylene-bridged analogue $3^{+\bullet}$, since the ($P/P^{+\bullet}$) redox centers in $1^{+\bullet}$ are significantly separated and lead to values of H_{IV} and λ that are similar to those in $2^{+\bullet}$. On the other hand,

(58) The activation free energy $\Delta G_{\text{EFF}}^\ddagger$ measured from the temperature dependence of the self-exchange rate constant is: $\Delta G_{\text{EFF}}^\ddagger = \Delta H_{\text{EFF}}^\ddagger - R\Delta S_{\text{EFF}}^\ddagger = 1.5 + 2.7 = 4.2 \text{ kcal/mol}$ at 295 K. This effective value is determined as the sum of the free energy of activation of ET ($\Delta G_{\text{ET}}^\ddagger$), precursor complex formation ($\Delta G_{\text{PC}} = -RT \ln K_{\text{PC}}$), and a term related to the temperature dependence of diffusion $\Delta G_{\text{diff}}^\ddagger$ (since reactions are close to the diffusion-controlled limit). That is, $\Delta G_{\text{EFF}}^\ddagger = \Delta G_{\text{ET}}^\ddagger + \Delta G_{\text{PC}} + \Delta G_{\text{diff}}^\ddagger$. From the experimentally determined: $\Delta G_{\text{EFF}}^\ddagger = 4.2$ and $\Delta G_{\text{PC}} = -0.9$, and taking into account the activation energy related to diffusion (which is: $\Delta G_{\text{diff}}^\ddagger \approx 2\text{--}3 \text{ kcal/mol}$ ^{58b}), the experimental barrier for ET can be estimated as: $\Delta G_{\text{ET}}^\ddagger(\text{exptl}) = \Delta G_{\text{EFF}}^\ddagger - \Delta G_{\text{PC}} - G_{\text{diff}}^\ddagger = 4.2 - (-0.9) - 2.5 = 2.6 \text{ kcal/mol}$, which agrees reasonably with the theoretical prediction from the Mulliken–Hush analysis: $\Delta G_{\text{ET}}^\ddagger(\text{theor}) = 2.5 \text{ kcal/mol}$. Note, however, that such a close coincidence may be somewhat fortuitous, since the accurate comparison requires the more rigorous estimate of diffusion effects. (b) Calvert, J. G.; Pitts, J. N., Jr. *Photochemistry*; Wiley: New York, 1966; p 627.

(59) In classical Marcus theory, reactants are surrounded by solvent that are rearranged to accommodate ET. The solvent (outer-sphere) reorganization is: $\lambda_{\text{out}} = e^2(1/D_{\text{op}} - 1/D_s)(1/2a_1 + 1/2a_2 - 1/r)$, where e is the charge transferred, D_{op} and D_s are the optical and static dielectric constants of medium, a_1 and a_2 are the radii of reactants, and r is the distance between them (as such, the decrease of r results in the diminution of solvent reorganization). It should be noted, however, that this relationship (or its modification, taking into account nonspherical shapes of the reactants) is (strictly speaking) valid only if: $r > (a_1 + a_2)$. Thus, it cannot be applied quantitatively to the pimer in which two phenothiazine moieties are positioned parallel to an interplanar separation less than their molecular size. As a result, the pimer is best considered as a dipole within the solvent sphere, and the redox process within such a pimer will require substantially less solvent reorganization.

(55) Since the electron-transfer self-exchange of organic cation radicals involve numerous molecular ($\sim 500\text{--}3000 \text{ cm}^{-1}$) and solvent ($\sim 10\text{--}100 \text{ cm}^{-1}$) vibrational modes, the pre-exponential factor $\nu_n = (\sum \nu_i^2 \lambda_i / \sum \lambda_i)^{1/2}$, as described by Sutin,² is difficult to rigorously calculate from the available data. Thus, for this study, we have simply taken ν_n to be uniformly 10^{12} s^{-1} , the same value as previously used for the description of ET in phenylene-bridged organic mixed-valence cation radicals³⁰ and in the kinetics evaluation of the intermolecular anion radical self-exchange.³⁷

(56) The ability of the two-state model to utilize the intervalence absorption bands to correctly predict the electron-transfer rates of mixed-valence cation radicals $1^{+\bullet}\text{--}3^{+\bullet}$ and (PH⁺/PH) self-exchange underscores its utilitarian value for further use provided that due cognizance is presently taken of the rigorous definitions of the separation parameter and the pre-exponential factor for reliable computations of the Mulliken–Hush electronic coupling element.

(57) Gramp, G.; Jaenicke, W. *Ber. Bunsen-Ges. Phys. Chem.* **1991**, *95*, 904.

the relative arrangement of (\mathbf{P}/\mathbf{P}^+) centers in the *o*-phenylene-bridged cation radical $\mathbf{3}^+$ is structurally quite related to that in the intermolecular pimer ($\mathbf{PH})_2^+$, and these closely related structures lead to intervalence absorption bands in the same NIR region and essentially the same reorganization energies. However, the electronic coupling element in $\mathbf{3}^+$ is almost twice that evaluated for the intermolecular pimer ($\mathbf{PH})_2^+$, and such a discrepancy in \mathbf{H}_{IV} may be related to the enhanced (electronic) interconnection of (\mathbf{P}/\mathbf{P}^+) centers in $\mathbf{3}^+$ that is abetted via an “unsaturated” bridge.

Summary and Conclusion

Analyses of the spectral (UV–NIR, ESR) and structural (X-ray crystallographic) data for the phenothiazine intermolecular pimer ($\mathbf{PH})_2^+$ and mixed-valence cation radicals $\mathbf{1}^+$, $\mathbf{2}^+$, and $\mathbf{3}^+$ yield considerable insight into the mechanism of intermolecular (ET) self-exchange in the following ways.

First: The precursor complex identified as the intermolecular pimer ($\mathbf{PH})_2^+$ must be explicitly included in the redox kinetics as described in Scheme 1 (eq 7). The Mulliken–Hush two-state model allows the critical electronic coupling element \mathbf{H}_{IV} and the Marcus reorganization energy λ to be evaluated via the intervalence (charge-resonance) absorption band, and the application of the Marcus–Hush eq 1 for the activation energy leads to the theoretical prediction of the ET rate that is in accord with that established experimentally via the temperature-dependent ESR line broadenings. The strong electronic coupling in the intermolecular pimer with $\mathbf{H}_{\text{IV}} = 660 \text{ cm}^{-1}$ results in substantial lowering of the activation barrier from (a) $\Delta G_{\text{ET}}^\ddagger = 4.2 \text{ kcal mol}^{-1}$ (in the absence of pimer) and ET rates that are rather slow on the ESR time-scale to (b) $\Delta G_{\text{ET}}^\ddagger = 2.1 \text{ kcal mol}^{-1}$ and ET rates at the diffusion-controlled limit. In other words, the intervention of the strongly coupled precursor complex ($\mathbf{PH})_2^+$ leads to ET rates of ($\mathbf{PH}/\mathbf{PH}^+$) self-exchange by two orders of magnitude faster than otherwise predicted solely from the value of the reorganization energy alone.^{60a}

Second: The intimate cofacial structure of the precursor complex ($\mathbf{PH})_2^+$ plays a critical role in increasing the magnitude of the electronic coupling and lowering the reorganization energy for the intermolecular ET,^{60b} and mechanistic insight is provided by the comparison of these ET parameters with those independently evaluated for the mixed-valence cation radical $\mathbf{1}^+$, $\mathbf{2}^+$, and $\mathbf{3}^+$. Thus, the electronic coupling within the intermolecular pimer ($\mathbf{PH})_2^+$ is comparable to that in the *o*-xylylene-bridged cation radical $\mathbf{2}^+$, but there are substantial differences in the reorganization energies that can be attributed to difference in the outer-sphere reorganization energies arising from slightly displaced (\mathbf{P}/\mathbf{P}^+) redox centers. On the other hand, the reorganization energy of the intermolecular pimer ($\mathbf{PH})_2^+$ is akin to that in the *o*-phenylene-bridged cation radical $\mathbf{3}^+$ in which (\mathbf{P}/\mathbf{P}^+) redox centers bear a close structural similarity, but different electronic coupling owing to an additional bridge connectivity.^{30b}

Third: As a prototypical redox center, phenothiazine is relevant to organic ET in general, especially insofar as the

strongly bonded precursor complex plays a critical role in ET kinetics. Thus, structural features of this intermolecular pimer, together with strong donor–acceptor coupling, result (a) the lowering of the classical Marcus activation barrier of $\Delta G_{\text{ET}}^\ddagger = \lambda/4$ by an amount \mathbf{H}_{IV} dictated by eq 1 and (b) the lowering of the reorganization energy relative to that predicted from the analysis of separated redox centers. The consequent lowering of the barrier for intermolecular ET differs dramatically to approach the diffusion-controlled limit despite a large reorganization energy that is either calculated theoretically or observed in the corresponding mixed-valence cation radical. For the mixed-valence cation radical to be an appropriate model for intermolecular ET the connecting bridge should allow the redox centers to adopt an appropriate face-to-face disposition without the introduction of an extraneous electronic connectivity.^{30b} The latter in a more extended context will provide the structural basis for the design of multicentered arrays consisting of substantially more than two redox centers to effect facile ET among polymolecular redox sites (i.e., electrical conductors, wires, etc.). We hope that further studies of other organic redox centers and different types of molecular bridges will provide more general support and extensions of these conclusions.

Experimental Section

Materials and Synthesis. Phenothiazine (Aldrich) was purified by recrystallization from benzene. Iodobenzene, 1,4-diiodobenzene, and *N*-methylphenothiazine (Aldrich) were used without further purification. Dichloromethane, acetonitrile, chloroform, toluene, hexane, and tetrahydrofuran were purified according to published procedures.⁶¹ 4,5-Dimethyl-1,2-diiodobenzene was synthesized by iodination of *o*-xylene with I_2 .⁶² 1,2-Bis(bromomethyl)methylbenzene was prepared by bromomethylation of benzenes.⁶³ Nitrosonium hexachloroantimonate was prepared from SbCl_5 and NOCl according to the literature procedure.⁶⁴ For the synthesis of 1,2-bis(phenothiazinyl-*N*-tolyl)benzene, the mixture of 398 mg (2 mmol) of phenothiazine and 10 mL of ethyl ether, 0.8 mL of 2.5 M *n*-butyllithium was added dropwise at room temperature with being stirred.⁶⁵ After 0.5 h, 132 mg (1 mmol) of 1,2-bis(bromomethyl)benzene in 5 mL of ethyl ether was added to the yellow solution. The mixture was stirred at room temperature for 1 h, and the precipitate was filtered and washed twice with 5 mL of ethyl ether. **2** (510 mg) was obtained (yield 66%) after recrystallization from dichloromethane/ethanol. The mononuclear donor **4** was synthesized in a similar manner with bromomethylbenzene. The attachment of the phenothiazine moiety to various benzene derivatives was achieved by the Ullmann arylation of phenothiazine with iodobenzenes.⁶⁶ For example, the mixture of phenothiazine (796 mg, 4 mmol), 1,4-diiodobenzene (660 mg, 2 mmol), potassium carbonate (3 g), and copper metal (100 mg) was heated at 220 °C for 3 days. After cooling, the solid was extracted with 100 mL of dichloromethane three times. The solvent was removed, and the residual was purified by chromatography over silica gel with dichloromethane/hexane (1/9) as elute. Recrystallization from dichloromethane/ethanol afforded 199 mg of **1** (20%). The mixed-valence donor **3** and the mononuclear donor **5** were synthesized by a similar procedure using 4,5-dimethyl-1,2-diiodobenzene and iodobenzene, respectively. All of the compounds prepared were characterized by ^1H NMR, ^{13}C NMR, MS, melting points, and

(60) (a) Note that the ET rate constant derived from classical Marcus theory [$Z \exp(-\lambda/4RT)$] is $k_{\text{ET}} = 8 \times 10^7 \text{ M}^{-1} \text{ s}^{-1}$ when $Z = 10^{11} \text{ M}^{-1} \text{ s}^{-1}$ and $\lambda = 17 \text{ kcal/mol}$. (b) The planarization of both phenothiazine redox centers in the pimer indicates that part of the reorganization energy is already taken up in the pre-equilibrium step prior to the electron-transfer step. Compare with: Gwaltney, S. R.; Rosokha, S. V.; Head-Gordon, M.; Kochi, J. K. *J. Am. Chem. Soc.* **2003**, *125*, 3273.

(61) Perrin, D. D.; Armarego, W. L. F.; Perrin, D. R. *Purification of Laboratory Chemicals*, 2nd ed.; Pergamon: New York, 1980.

(62) Hart, H.; Harada, K.; Du, C.-J. *F. J. Org. Chem.* **1985**, *50*, 3104.

(63) Závada, J.; Pánková, M.; Aenold, Z. *Collect. Czech. Chem. Commun.* **1976**, *41*, 1777.

(64) Kim, E. K.; Kochi, J. K. *J. Am. Chem. Soc.* **1991**, *113*, 4962.

(65) Clarke, D.; Gilbert, B. C.; Hanson, P.; Kirk, C. M. *J. Chem. Soc., Perkin Trans. 2* **1978**, *10*, 1103 and references therein.

(66) Okada, K.; Imakura, T.; Oda, M.; Murai, H. *J. Am. Chem. Soc.* **1996**, *118*, 3047.

elemental analysis, as follows. 1,2-Bis(phenothiazinyl-*N*-tolyl)benzene (**2**): mp 218 °C dec; yield 66%. ¹H NMR (CDCl₃): δ 7.34 (m, 2H), 7.19 (m, 2H), 7.10 (d, *J* = 8.4 Hz, 4H), 7.00 (m, 4H), 6.90 (m, 4H), 6.67 (d, *J* = 8.4 Hz, 4H), 5.23 (s, 4H). ¹³C NMR (CDCl₃): δ 144.1, 133.6, 129.2, 128.2, 127.2, 127.0, 123.7, 122.6, 121.3, 115.5, 50.5. Anal. Calcd for C₃₂H₂₄N₂S₂: C, 76.80; H, 4.80. Found: C, 76.78; H, 4.89. 1,4-Bis(*N*-phenothiazinyl)benzene (**1**): mp 250 °C dec; yield 20%. ¹H NMR (CDCl₃): δ 7.51 (s, 4H), 7.14 (d, *J* = 7.8 Hz, 4H), 7.00 (t, *J* = 7.2 Hz, 4H), 6.93 (t, *J* = 7.2 Hz, 4H), 6.53 (d, *J* = 7.8 Hz, 4H). ¹³C NMR (CDCl₃): δ 143.0, 140.3, 130.3, 127.1, 126.9, 123.2, 122.7, 117.8. Anal. Calcd for C₃₀H₂₀N₂S₂: C, 76.27; H, 4.24. Found: C, 75.85; H, 4.26. 1,2-Bis(*N*-phenothiazinyl)4,5-dimethylbenzene (**3**): mp 225 °C; yield 26%. ¹H NMR (CDCl₃): δ 7.53 (s, 2H), 6.75 (m, 4H), 6.53 (m, 8H), 6.11 (m, 4H), 2.49 (s, 6H). ¹³C NMR (CDCl₃): δ 144.1, 140.2, 133.6, 129.0, 128.2, 127.1, 123.7, 122.6, 115.6, 16.5. Cyclic voltammetry was performed on a BAS 100A Electrochemical Analyzer as described previously.³⁰

Isolation of Cation Radical and Dication Salts. Addition of 1 equiv NOSbCl₆ (or NOPF₆) to the phenothiazines **PH** and **PMe**, the mixed-valence donors **1**, **2**, and **3**, or the mononuclear models **4** and **5** in dichloromethane at -40 °C produced dark red solutions of the cation radicals. After removal of NO (gas), hexane was added, and the dark red precipitate of the cation radical was filtered and washed with cold hexane. Mixed-valence dications **1**²⁺, **2**²⁺, and **3**²⁺ were similarly produced using 2:1 molar ratio of nitrosonium to the bridged donor. The purities of all salts were determined by iodometric titration and were found to be greater than 98%.⁶⁷

UV-vis-NIR spectroscopic measurements were carried out with a Cary 500 UV-vis-NIR spectrometer. The pure, isolated salt of the mononuclear or mixed-valence cation radicals (or dications) was dissolved in dichloromethane in a Schlenk tube and transferred under an argon atmosphere into the quartz spectroscopic cell (equipped with a Teflon valve fitted with Viton O-rings). The samples of cation radical salts (KBr pellets) for solid-state (UV-vis-NIR) absorption measurements were prepared under an argon atmosphere in a glovebox.

UV-Vis-NIR Study of Phenothiazine Pimer Formation. The phenothiazine donor **PH** and its cation radical **PH**^{•+} were characterized in dichloromethane solution by intense absorption bands in the UV region. The cation radical additionally showed absorption bands in the visible region with major peaks at 437 and 519 nm and in NIR region with peaks at 664, 729, and 820 nm (Table 1). (Note that cooling the concentrated solution of cation radical **PH**^{•+} led to the appearance of new absorption band at ~700 nm because of the formation of cation radical dimer (**PH**)₂²⁺ as illustrated in Figure S6.) When phenothiazine **PH** was added to the solution of cation radical **PH**^{•+}, a new (Gaussian) band centered at 1600 nm appeared (Figure 1), consistent with the dynamic association of the electron donor with its cation radical (i.e., pimer formation).³⁷ From the absorbance dependence of this band on the concentration of **PH**, the pimer formation constant and extinction coefficient of new band were determined by the Benesi-Hildebrand procedure (see text).

The spectral characteristics of mixed-valence cation radicals **1**^{•+}–**3**^{•+} in the UV-vis region were similar to those of their mononuclear cation radicals **4**^{•+} and **5**^{•+} and phenothiazine cation radical **PH**^{•+}. Spectral analysis of the mixed-valence cation radicals **1**^{•+}–**3**^{•+} via oxidative titration of the parent donor with SbCl₅ revealed the intervalence bands, as follows. The addition of 0.5 mM oxidant to 2 mM solution of donor **1** resulted in the appearance of absorptions corresponding to local bands of phenothiazine cation radical (maxima at 680, 780, and 880) and an extra component as a shoulder around 900–1100 nm (Figures 3B). Increasing concentrations of the oxidant led to a linear growth of intensity of all bands until concentration of oxidant reached that of donor **1**. With further additions of oxidant, the

(local band) maxima at 780 and 880 nm continued to rise, but the intensity of low-energy shoulders dropped, and a well-defined isosbestic point was observed (Figure 3B). Finally, when the concentration of the oxidant to bridged donor attained a 2:1 molar ratio (i.e., the oxidant concentration equal to the concentration of phenothiazine redox centers **P**), the spectral shape became quite close to that of mononuclear cation radical **5**^{•+} (Table 1). Such a spectral behavior indicated that the low-energy component was related to the presence of both neutral and cationic counterparts within the bridged species, i.e., it was the intervalence transition. (The addition of the neutral donor **1** to the solution of cation radical **1**^{•+} did not alter the electronic spectrum in the NIR range, which confirmed the *intramolecular* nature of the NIR absorption.) Digital deconvolution of the NIR absorption into Gaussian components led to the parameters (wavelength and ε) of the intervalence bands of **1**^{•+} listed in Table 1. The mixed-valence donor **2** showed essentially the same spectral behavior (Figure S5), and spectral deconvolution of mixed-valence cation radical **2**^{•+} (inset in Figure S5) afforded spectral parameters in Table 1.

The addition of the oxidant to 2 mM solution of **3** resulted in the appearance of bands in the 700–900 nm range and a new band at ~1700 nm (Figure 3A). The intensity of all of the NIR absorption bands grew linearly with concentration of oxidant until the molar ratio of the oxidant to that of the neutral donor approached 1:1. Further additions of oxidant led to the gradual disappearance of the band at 1700 nm, while the intensity of absorption in the 700–900 nm range continued to grow (although the shape of the spectra changed significantly relative to that of model cation radical **5**^{•+}; Figure 3A). Finally, when the concentration of oxidant reached twice that of the initial concentration of donor **3**, the low-energy band at ~1700 nm disappeared, and a single, very intense band with maximum at 700 nm was observed in the 600–900 nm spectral range. We thus assigned the absorption band at 1700 nm to the intervalence band of mixed-valence cation radical **3**^{•+}. (The energy of this band was solvent-dependent (Table S1), whereas the positions of the local bands were essentially invariant.) The intense absorption band of dication **3**²⁺ at 700 nm was reminiscent of that observed in phenothiazine dimer and was attributed to the strong interaction of phenothiazine cation radical centers in the formation of the diamagnetic dication.^{23,25}

ESR measurements (from -90 to +30 °C) were performed on Bruker ESP-300 X-band or Varian E-line Century 100 ESR spectrometer as described.^{25,30} ESR spectra simulations (PEST WinSim program, V. 0.96, Public EPR Software Tools, National Institute of Environmental Health Sciences) were carried out as described earlier.³⁰ The intramolecular ET rate constants *k*_{ET} within mixed-valence cation radical **1**^{•+}, **2**^{•+}, and **3**^{•+} were evaluated from the temperature-dependent line broadening using dynamic ESR spectra simulations (ESR-EXN program) as described previously.^{30,32} The intermolecular self-exchange rate constants *k*_{SE} (for **PH**^{•+}/**PH** and **PMe**^{•+}/**PMe** dyads in dichloromethane) were determined from the dependence of cation radical ESR line widths on concentration of parent donor in the fast-exchange limit.¹⁴ The ESR spectrum of phenothiazine cation radical (Figure S1) changed dramatically upon addition of parent phenothiazine. Initially, the well-resolved spectrum broadened to the four unresolved lines (Figure S2), and then the incremental addition of phenothiazine gradually led to single broad line. This broad line became narrower with the continuous addition of the neutral donor, i.e., system approached the fast-exchange limit. Following earlier studies,¹⁴ the electron self-exchange rate constant *k*_{SE} was calculated in fast-exchange limit from the slope of dependence of line width (Δ*H*) on the inverse concentration of the parent donor, 1/*C* (Figure S3) as *k*_{SE} = 2.05 × 10⁷∇/slope, where ∇ is the second moment of the ESR spectrum.¹⁴ The same procedure was carried out at different temperatures, and Arrhenius dependence of rate constants (Figure S4) led to the activation energy *E*_a and pre-exponential factor (log *A*).

X-ray Crystallography of the Cation Radicals. The intensity data were collected with aid of a Siemens SMART Apex diffractometer equipped with a CCD detector using Mo Kα radiation (λ = 0.71073

(67) Rathore, R.; Kumar, A. S.; Lindeman, S. V.; Kochi, J. K. *J. Org. Chem.* **1998**, *63*, 5847.

Table 7. Crystallographic Data for Aromatic Donors and Their Cation Radicals

| | 1 | 1 ⁺ SbF ₆ 2CH ₂ Cl ₂ | 2 | 2 ⁺ CB ₁₁ (CH ₃) ₁₂ ⁻ 2CH ₂ Cl ₂ | 3 | (PH) ₃ ²⁺ PH (PF ₆ ⁻) ₂ |
|--|---|---|---|--|---|--|
| empirical formula | C ₃₀ H ₂₀ N ₂ S ₂ | C ₃₂ H ₂₄ Cl ₄ F ₆ N ₂ S ₂ Sb | C ₃₂ H ₂₄ N ₂ S ₂ | C ₄₇ H ₆₄ B ₁₁ Cl ₄ N ₂ S ₂ | C ₃₂ H ₂₄ N ₂ S ₂ | C ₄₈ H ₃₆ F ₁₂ N ₄ P ₂ S ₄ |
| fw | 472.60 | 878.20 | 500.65 | 981.83 | 500.65 | 1086.98 |
| cryst syst | orthorhombic | triclinic | triclinic | monoclinic | tetragonal | monoclinic |
| space group | <i>Pbca</i> | <i>P1</i> | <i>P1</i> | <i>P2₁/c</i> | <i>I₄/a</i> | <i>C2</i> |
| <i>a</i> , Å | 13.869(1) | 7.782(1) | 10.764(1) | 14.695(1) | 13.819(1) | 19.303(1) |
| <i>b</i> , Å | 8.0185(4) | 10.292(1) | 12.195(1) | 23.991(1) | 13.819(1) | 11.225(1) |
| <i>c</i> , Å | 20.090(1) | 10.450(1) | 19.820(1) | 15.625(1) | 26.189(2) | 20.546(1) |
| α, deg | 90 | 96.32(1) | 107.86(1) | 90 | 90 | 90 |
| β, deg | 90 | 99.68(1) | 96.35(1) | 110.95(1) | 90 | 92.84(1) |
| γ, deg | 90 | 94.16(1) | 95.02(1) | 90 | 90 | 90 |
| <i>V</i> , Å ³ /Z | 2234.1(2)/4 | 816.5(1)/1 | 2440.6(1)/4 | 5144.5(4)/4 | 5001.6(5)/8 | 4446.3(4)/4 |
| ρ _{calcd} , g/cm ³ | 1.405 | 1.768 | 1.363 | 1.268 | 1.330 | 1.624 |
| total/unique reflns | 24484/3685 | 9002/5096 | 26742/15165 | 48067/12777 | 27473/4238 | 24530/7549 |
| data [<i>I</i> > 2σ(<i>I</i>)] | 3268 | 4484 | 12585 | 8571 | 3256 | 6455 |
| <i>R</i> ₁ ^a / <i>wR</i> ₂ ^b | 0.041/0.108 | 0.035/0.082 | 0.048/0.114 | 0.065/0.149 | 0.056/0.144 | 0.061/0.152 |

$$^a R_1 = \sum ||F_o| - |F_c|| / \sum |F_o|, \quad ^b wR_2 = \{ \sum [w(F_o^2 - F_c^2)^2] / \sum [w(F_o^2)^2] \}^{1/2}$$

Å) at -150 °C unless otherwise specified. The structures were solved by direct method and refined by full matrix least-squares procedure with IBM Pentium and SGI O₂ computers.⁶⁸ The X-ray structure details of compounds mentioned here are on deposit and can be obtained from Cambridge Crystallographic Data Center, 12 Union Road, Cambridge, CB2 1EZ U.K.

Single crystals of the neutral mixed-valence donors **1**, **2**, and **3** were obtained by the slow evaporation of their solutions in dichloromethane/ethanol mixture. To obtain single crystals of mixed-valence cation radical **1**⁺, a solution of (2 mM) nitrosonium hexachloroantimonate (NO⁺SbCl₆⁻) and donor **1** (2 mM) in dichloromethane (20 mL) was prepared under an argon atmosphere at -30 °C. The solution was carefully layered with toluene and placed in the cold bath (-60 °C). After 7 days, the dark red single crystals were formed as the cation radical salt (**1**⁺ SbCl₆⁻) suitable for X-ray crystallographic analysis. The single crystals of the mixed-valence cation radical **2**⁺ were obtained by the exposure of the neutral donor **2** (4 mmol) with 1 equiv of decamethylcarbonyl radical in dichloromethane at 23 °C. Careful layering of this solution with hexane followed by refrigeration at -65 °C for 2 weeks afforded dark red crystals of **2**⁺ CB₁₁(CH₃)₁₂⁻. The single crystals of the dication **2**²⁺(SbCl₆⁻)₂ were obtained by oxidation of **2** with 2 equiv of tris(4-bromophenyl)aminium hexachloroantimonate in dichloromethane, followed by crystallization as described earlier. To obtain single crystals of phenothiazine pimer, the 4-fold excess of phenothiazine donor was added to 1,2-dichloroethane solution of pure phenothiazine cation radical salt **PH**⁺PF₆⁻. Careful layering of this solution with *n*-hexane and refrigeration at -30 °C for 2 weeks afforded well-formed dark brown prisms, with the overall stoichiometric [1:1] composition (**PH**⁺PF₆⁻)(**PH**). Crystallographic data for the pertinent aromatic donor, their cation radicals, dications, and pimer are presented in Table 7.

Acknowledgment. We thank Professor S. F. Nelsen for kindly providing us with a copy of the ESR-EXN program, J. M. Lu

for help with some of the ESR spectral measurements, S. V. Lindeman for crystallographic assistance, and the R. A. Welch Foundation for financial support.

Supporting Information Available: Solvent dependence of the intervalence band for the mixed-valence cation radical **3**⁺ (Table S1), selected bond lengths and angles from X-ray studies of phenothiazine-based systems (Table S2), ESR spectra (experiment and simulation) for the cation radical **PH**⁺ (Figure S1), concentration effects of the parent donor **PH** on line shape of cation radical **PH**⁺ ESR spectrum (Figure S2) and its line width Δ*H* (Figure S3), Arrhenius dependence of the self-exchange rate constant for **PH**⁺/**PH** dyad (Figure S4), solid-state spectrum of phenothiazine pimer (Figure S5), temperature dependence of the electronic spectrum of concentrated solutions of phenothiazine cation radical in dichloromethane (Figure S6), spectral changes upon oxidative titration of the mixed-valence donor **2** (Figure S7), ESR spectra (experiment and simulation) for the mononuclear cation radical **5**⁺ (Figure S8), temperature-dependent ESR spectra of mixed-valence cation radical **2**⁺ and dynamic ESR simulation (Figure S9), ORTEP diagram for the donor **3** from X-ray crystallography (Figure S10), ESR spectra of dication diradicals **1**²⁺ and **2**²⁺ (Figure S11), and ORTEP diagram of the dication salt **2**²⁺(SbCl₆⁻)₂ (Figure S12) (PDF, CIF). This material is available free of charge via the Internet at <http://pubs.acs.org>.

JA038746V

(68) Sheldrick, G. M. *SHELXS-86, Program for Structure Solution*; University of Göttingen: Göttingen, Germany, 1986.